Searching for Persistent Radio Sources

Thesis by
Jerome Seebeck

In Partial Fulfillment of the Requirements for the
Degree of
Bachelor of Science in Astrophysics

CALIFORNIA INSTITUTE OF TECHNOLOGY
Pasadena, California

2022
Defended June 4th, 2022

Jerome Seebeck
ORCID: 0000-0002-4014-9067

ACKNOWLEDGEMENTS

Firstly I would like to thank my family: my three brothers Lyle, Ray, Henry and my mom and dad for their support in my academic journey (especially during my time spent at home and hopping across the west coast my junior year).

I would like to thank my thesis advisors Vikram Ravi and Casey Law. Thank you Vikram for a wonderful introduction into astronomy during Ay 20 and for taking me on as a SURF student in 2021. Your guidance in every research meeting and throughout the writing process of my first paper was vital in this project. Thank you Casey for helping the entire way through this project from helping me figure out what PRS are to helping me run code, this thesis would not have been possible without you. Thank you both for your guidance and recommendations through the graduate school admissions process. I would also like to thank the rest of my thesis advising committee Liam Connor and Dana Simard for their help throughout the way.

Outside of the immediate thesis research group there are so many people that helped this work. I want to thank Lynne Hillenbrand for getting me started in astronomy research on FU Ori stars and helping with grad school admissions. I want to thank my advisor Andrew Howard for helping with my courses. I also want to give a big thank you to my friends without whom I would not have made it through this school: Steve, Gokul, Riley, Noah, Ethan, and my girlfriend Rae.

Lastly, thank you mom, for inspiring me to pursue astronomy. I wish you were here to see it.

ABSTRACT

We present a sample of 27 sources from the Very Large Array Sky Survey (VLASS) associated with dwarf galaxies as possible persistent radio sources (PRS). This thesis presents a novel approach of high offset associations between radio sources and optical counterparts from the Galaxy List for the Advanced Detector Era+ (GLADE+) through the use of the Bayesian association algorithm Probabilistic Association of Transients to their Hosts (PATH). We follow up on this sample with SED fitting through UV, optical, and IR photometry to garner accurate star formation and stellar masses for the sample. We use this data to search for high luminosity (excess $L_\nu \geq 10^{29} erg\, s^{-1}\, Hz{-}1$), high offset (> 2"), and high association probability ($P(O|x) \geq 0.93$) sources for follow up. Our goal for further follow up is to eliminate possible astrophysical foreground such as AGN, SNe, and star formation as explanation for these sources. We follow up with Keck Low Resolution Imaging Spectrometer (LRIS) optical spectra of 2 sources and find no evidence of AGN activity. We also discuss our VLBA proposal for 11 of our sources to search for compactness of source radio emission, a feature of PRS. Additional follow up spectroscopy and radio observations are necessary to confirm any of these candidates and PRS due to the large number of foregrounds and this thesis presents a possible list of 27 candidates within VLASS in order to do so.

TABLE OF CONTENTS

LIST OF ILLUSTRATIONS

LIST OF TABLES

NOMENCLATURE

Active Galactic Nuclei. Active supermassive black holes at the center of galaxies that emit bright jets and winds, and shape their galaxies.

False negatives (FN). Where the correct galaxy is identified by PATH with association probability below 0.9.

False Positive Rate. $\frac{FP}{FP+TN}$.

False positives (FP). The PATH association was secure but the identified host galaxy was incorrect.

Fast Radio Burst. Extragalactic, sub-millisecond radio impulses of unknown origin.

Persistent Radio Source. Luminous radio sources that are not variable with respect to time and have been linked with FRBs.

Spectral Energy Distribution (SED). Plot of energy vs frequency or wavelength for an astronomical source, which can be used to classify and determine characteristics of that source..

True negatives (TN). Where an incorrect host galaxy is preferred by PATH with association probability below 0.9..

True Positive Rate. $\frac{TP}{TP+FN}$.

True positives (TP). We correctly identify the host when accepting the PATH association.

Chapter 1

MOTIVATION AND BACKGROUND

1.1 Fast Radio Bursts

Since the confirmed discovery of the first Fast Radio Burst (FRB) in 2013 (Lorimer et al., 2007; Thornton et al., 2013), the science around these transients has boomed. According to the NASA ADS archive in the year of their discovery there were 5 refereed papers published on the topic, 8 years later in 2021 there were 191 refereed papers. The search for these extragalactic millisecond transients has captured the interest of theorists and observers alike. Leading theories for the origins of these sources are centered around magnetars, but the question of how these compact objects are able to produce these high energy bursts remains open. Next generation wide field instruments such as the Canadian Hydrogen Intensity Mapping Experiment (CHIME) and Deep Synoptic Array (DSA) have recently been brought online with the intended purpose of searching and localizing these transients. To date nearly 1000 FRBs have been observed (Mandana Amiri et al., 2021; Cordes and Shami Chatterjee, 2019; Lorimer et al., 2007; Petroff, Hessels, and Lorimer, 2019). With a characteristic fluence of 1 Jy ms and redshift $z \sim 0.1$, FRBs have an isotropic-equivalent energy of 2×10^{29} erg s^{-1} Hz^{-1}, orders of magnitude larger than pulses from pulsars.

Roughly ten percent of the FRB population are known to emit multiple bursts (e.g., CHIME/FRB Collaboration, Andersen, et al., 2019). The discovery of repeating FRBs has had a large impact on the question of FRB origin, because they demonstrate that some bursts are not cataclysmic (Spitler et al., 2016). However, it is not clear whether all FRBs repeat or if repetition is a hallmark of a subclass of FRBs (Vikram Ravi, 2019). There is some evidence that repetition is a hallmark of a subclass of FRBs, as the burst spectra are wider in duration and narrower in bandwidth than bursts from non-repeating FRBs (Pleunis et al., 2021). However, there is no evidence that host galaxies properties differ between repeating and non-repeating FRBs (Bhandari et al., 2022a). More than twenty FRBs have been localized to arcsecond precision and associated with a host galaxy with a spectroscopic distance (Bannister et al., 2019; Heintz et al., 2020; Marcote, Nimmo, et al., 2020; V. Ravi et al., 2019). This sample of FRBs has been used to characterize the stellar

environment of FRBs (Mannings et al., 2021; Shriharsh P. Tendulkar et al., 2021), study the FRB local magneto-ionic environment (Hilmarsson et al., 2021; Michilli et al., 2018), and measure the baryon density of the intergalactic medium (Macquart, Prochaska, et al., 2020).

A massive global effort is underway to design telescopes and instruments to detect, localize, and characterize FRBs (Mandana Amiri et al., 2021; CHIME/FRB Collaboration, M. Amiri, et al., 2019; Kocz et al., 2019; Law, Bower, et al., 2018; Macquart, Bailes, et al., 2010; Rajwade et al., 2021; Venkatraman Krishnan et al., 2020). Determining the source(s) of FRBs is a central motivation in this effort. One approach is to identify a large sample of FRB host galaxies to compare the event rate/density and offset distribution potential progenitor classes (Bhandari et al., 2022b). Another approach is to characterize individual FRBs in detail to test formation scenarios and emission models, such as has been done with FRBs associated to a magnetar and a globular cluster (Bochenek et al., 2020; Kirsten et al., 2021). Understanding the source model is critical to using FRBs as probes of extragalactic gas or for precision cosmology, since some FRBs (e.g., FRB 20121102A) are known to live in messy environments or have complex burst spectra that confound their use as probes. The scope for this application is potentially huge, including measuring the local baryon density (Macquart, Prochaska, et al., 2020), the expansion rate of the universe (Wu, Yu, and Wang, 2020), and searching for primordial black holes via gravitational lensing (Eichler, 2017). Characterizing and classifying FRBs will be crucial for next-generation applications.

1.2 Persistent Radio Sources

Eight repeating FRBs have been localized precisely enough to be associated with multiwavelength counterparts (Heintz et al., 2020; Marcote, Nimmo, et al., 2020; Vikram Ravi et al., 2021). Two, highly-active repeating FRBs, 20121102A and 20190520B, are noteworthy for having burst properties and multiwavelength associations that make then near twins (Figure 1.1). Both FRBs are coincident with luminous, persistent radio sources (PRS) of unknown origin (S. Chatterjee et al., 2017; Niu et al., 2021). Both FRBs also reside in low-metallicity dwarf galaxies with high specific star formation rates ($M_* \approx 10^8 M_\odot$, SFR $\approx 0.5\, M_\odot\, yr^{-1}$; S. P. Tendulkar et al., 2017). One possibility is that the PRS and host galaxy environment are signatures of a special subclass of FRB (Niu et al., 2021, Tsai et al, in prep).

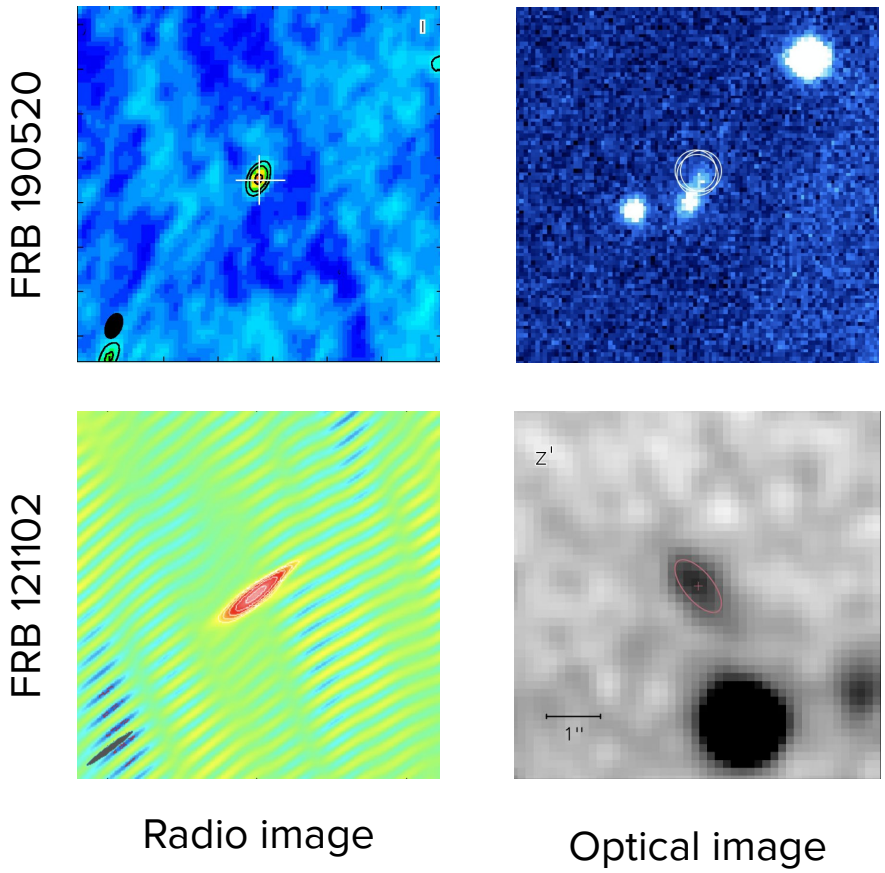

Figure 1.1: Grid of radio and optical images of FRBs 20121102A and 20190520B. Both are associated with dwarf galaxies and compact, persistent radio sources (PRS).

The two[1] confirmed PRS have a radio luminosity $L_r \approx 3 \times 10^{29}\, erg\, s^{-1}\, Hz^{-1}$, comparable to the luminosity of AGN. The incoherent synchrotron radiation has been modeled to estimate its size, age, and how it is energized. (Katz, 2021; Margalit and Metzger, 2018; Murase, Kashiyama, and Mészáros, 2016). The PRS associated with FRB 20121102A has an electron density of 10^2 cm^{-3} with a ~mG magnetic field contained in a size smaller than 0.7 pc (Marcote, Paragi, et al., 2017; Michilli et al., 2018). Similar constraints have been made for the PRS in FRB 20190520B (Yu et al., in prep; Ocker et al., in prep; Thomas et al., in prep). Despite these physical constraints, it is not known what kind of source generates either FRBs, PRS, or why they are related. Thus PRS are key to understanding the origin and classification of FRBs. The two known PRS have helped constrain

[1] A candidate PRS was recently published in Chibueze et al. (2021), however it is not yet known that the emission is compact (pc-scale).

physical conditions in their environment, but more examples are needed to interpret correlations with properties such as FRB activity. Law, Connor, and K. Aggarwal (2021) present a statistical test of whether PRS are preferentially associated with repeating FRBs. While the test is not yet conclusive, increasing the sample by 20% may be sufficient to show that PRS do prefer repeating FRBs.

1.3 Active Galactic Nuclei

Independent of the FRB field, the PRS phenomenon confounds the study of AGN in the local universe. Recently, Reines, James Condon, et al. (2020) identified dozens of luminous radio sources in dwarf galaxies that are presumed to be supermassive black holes (Greene and Ho, 2007; Reines and Volonteri, 2015). Some of these sources are non-nuclear "wandering black holes" that are expected signatures of a recent galaxy merger. However, Eftekhari et al. (2020) noted the phenomenological similarity of the PRS with AGN. The PRS volumetric density is also consistent with that estimated for the wandering black hole sample ($4 \times 10^2\ Gpc^{-3}$; Eftekhari et al., 2020; Law, Connor, and K. Aggarwal, 2021)

The ambiguity between AGN and PRS (Chen, Vikram Ravi, and Hallinan, 2022) argues for caution when classifying based on radio data alone. Nuclear radio sources are likely to be AGN and off-nuclear radio sources may be a PRS, but gas dynamics and ionization are required to show that definitively. Given the similar number density of PRS and AGN in dwarf galaxies, it is likely that PRS have already been detected and perhaps misidentified as AGN in deep radio surveys (M. Mezcua, Suh, and Civano, 2019). This confusion must be resolved in order to use local AGN to study black hole formation and feedback.

1.4 Contributions of this Thesis: Searching for PRS

This thesis is motivated by the recognition that PRS constitute a significant new class of extragalactic radio source. Law, Connor, and K. Aggarwal (2021), used the FRB repetition statistics to estimate a FRB *source* density. Given the occurrence rate of PRS in FRBs, we can then estimate a volumetric density of PRS in the local universe of $\mathcal{N}_{PRS} \approx 50 - 10000\ f_{b,0.1}^{-1}$ Gpc^{-3}, assuming a pulsar-like FRB beaming fraction. With this density and characteristic PRS luminosity of $10^{29}\ erg\ s^{-1}\ Hz^{-1}$, the Very Large Array Sky Survey (VLASS) will detect $4 - 830$ PRS out to a distance of $z = 0.065$ (luminosity distance of 300 Mpc). In a volume limited sample of radio sources in the local universe, PRS potentially amount to as much 1% and 7% of the AGN and star-forming galaxy populations, respectively.

Given the occurrence rate of PRS it is likely that PRS have already been detected and misidentified (Law, Connor, and K. Aggarwal, 2021). The growth of all-sky surveys in astronomy has caused a data boom. Terabytes of astronomical information are being gathered from the sky each night. This is too much data to be observed by humans and although machine learning algorithms are becoming stronger, identifying a new subclass of objects like PRS is incredibly difficult. We will identify a list of PRS candidates for additional follow up through archival searches of numerous catalogs. Chapter 2 will outline the process for gathering initial sources, their host galaxies, SED fitting, and a refined source list. Chapter 3 describes our follow up optical spectroscopy observations and proposed VLBA observations. Chapter 5 provides a summary and final candidate list.

Chapter 2

CONSTRUCTING AN INITIAL PRS CANDIDATE LIST

2.1 Overview and PRS Characteristics

This chapter aims to show the methods for creating an initial candidate list for PRS associated with host galaxies. We suggest defining a PRS as an FRB associated radio source with a spectral luminosity $L_\nu > 10^{29} erg\, s^{-1}\, Hz^{-1}$ that is not attributed to star-formation activity in the host galaxy. This is a value adopted by Law, Connor, and K. Aggarwal (2021) as it is higher than most supernovae (SNe), HII regions, and other astrophysical foregrounds. However, this can not be used to rule out AGN as they can be this luminous. Thus we can use $L_\nu > 10^{29} erg\, s^{-1}\, Hz^{-1}$ to select for possible AGN and PRS and eliminate AGN with further analysis. It is also worthwhile to note that this cutoff is not a requirement for PRS. A PRS could exist with a lower luminosity but this cutoff is especially useful for eliminating astrophysical foregrounds like SNe. We also consider the PRS volumetric rate in the local universe estimated by Law, Connor, and K. Aggarwal (2021) of $\mathcal{N}_{PRS} \approx 50 - 10000\, f_{b,0.1}^{-1}$ Gpc^{-3}. According to this definition deep radio source catalogs with large sky coverage will have detected PRS.

2.2 Cross matching VLASS and GLADE

The first step in our archival data reduction is to cross-match a radio and optical catalog. Radio sources with optical counterparts are ideal for multiwavelength follow up. As the radio source and optical detection can allow us to gleam different information about these sources. As a radio catalog, we used an all-sky 3 GHz source catalog from epoch 1.2 and 2.1 image data (using pipeline and corrected astrometry, as described in Dong et al., 2021) from VLASS. This catalog surveys the entire sky north of -40 degrees at a resolution of 2.5" with a 1 sensitivity of 70 μJy/beam, at a frequency of 3 GHz totaling nearly 1.4 million sources. This large amount of coverage, high sensitivity, and fantastic spatial resolution make the VLASS a ideal catalog for PRS searches. For our optical galaxy catalog we decided to use the Galaxy List for the Advanced Detector Era+ (GLADE+) (Dálya et al., 2021). This is a local universe galaxy catalog which combines 6 separate but not necessarily independent catalogues. The catalog contains 22.5 million sources and is 90 percent complete up to 500 Mpc. The overlapping sky coverage for these

catalogs can be seen in (Figure 1.1), while not perfect a majority of both of the catalog survey areas overlap.

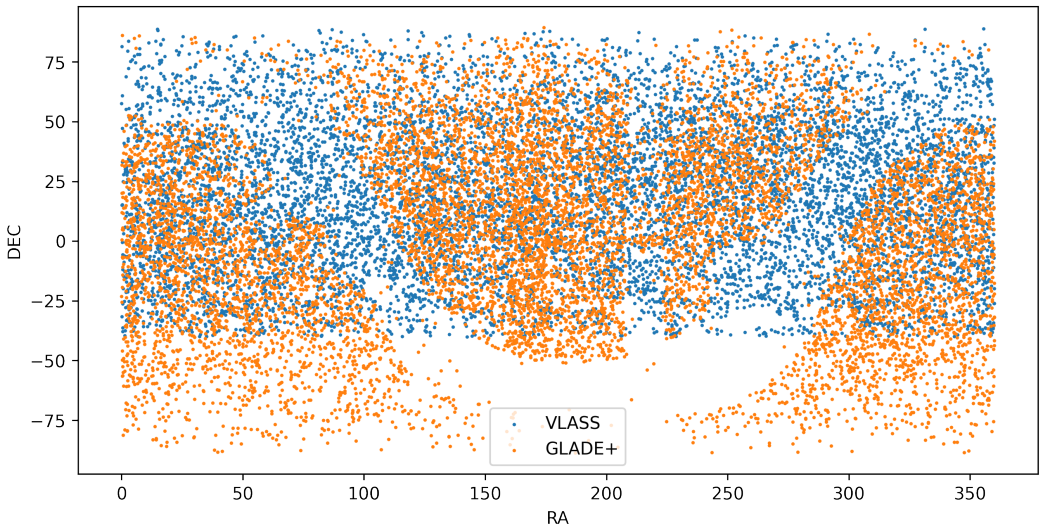

Figure 2.1: Sky coverage map for GLADE+ (orange) and VLASS (blue). VLASS covers the entire northern sky north of -40 degrees in the radio. GLADE+ is a local galaxy catalog that covers the entire sky outside of the plane of the Milky Way.

The previously mentioned Reines, James Condon, et al. (2020) followed a similar procedure but instead cross matched the NASA-Sloan Atlas with the VLA Faint Images of the Radio Sky at Twenty centimeters (FIRST) Survey. Thus there should be some overlap in sources which can be used to check our methods and results. Due to the occurrence of both PRS associated with FRB 20121102A and 20190520B in dwarf galaxies we provided a cut on the GLADE+ catalog to limit the sample to dwarf galaxies. We take the cuts as described in Reines, James Condon, et al. (2020) selecting sources with $M_* < 3\ X\ 10^9 M_\odot$ which is approximately equal to the mass of the Large Magellanic Cloud (LMC). Mass estimates from GLADE+ are derived from mass to light ratios in the infrared WISE W1-band. Our dwarf galaxy sample has 390,533 sources with a minimum stellar mass of $3 \times 10^7 M_\odot$.

We then proceed to cross correlate our GLADE+ dwarf galaxy catalog with VLASS up to a match radius of 30". This radius provides us ample range to detect sources that are offset from galaxies with larger angular sizes. The angular offset of these sources can be seen as the blue distribution in (Figure 2.2). After cross match we reported 2767 VLASS sources within 30" of a GLADE source. Typical literature (Reines, James Condon, et al., 2020) from this point on would provide a cut at around 5" as much of the rise after that point is likely due to chance alignment. However

that method likely excludes a subset of true associations that are extremely offset from their host or sources in galaxies with large angular sizes: prime candidates for PRS. Instead for this manuscript we decided to use a new method: Probabilistic Association of Transients to their Hosts (PATH; Kshitij Aggarwal et al., 2021). This is a Bayesian algorithm that calculates the chances of association with specific galaxies, given a set of priors on the nature of source progenitors and their locations in galaxies. The priors include information on the nature of the host galaxies, the distributions of projected physical offsets, the probability of the host galaxy being unobserved in the galaxy catalogue, and the source localization ellipse. The ability of PATH to weight probabilities between different galaxies, consider a diverse set of priors, and consider unseen galaxies, makes it a much more robust tool for our work.

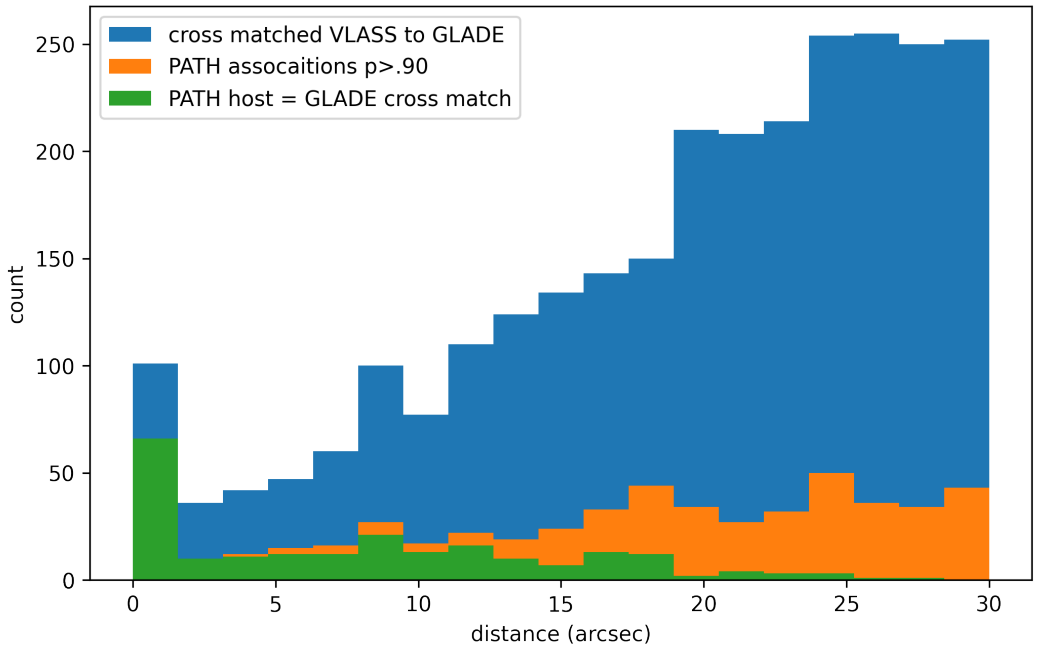

Figure 2.2: Distributions for the different steps along the PRS candidate pipeline in Chapter 2. The blue distribution shows the initial cross-match between VLASS and GLADE+, the orange distribution shows all cross-matched candidates with association probabilities above 90%, and the green distribution shows positively associated PATH candidates whose chosen host is associated with the original GLADE+ source.

2.3 PATH PS1 Associations

Constructing a Galaxy Catalog

For each VLASS source within 30 of a GLADE+ galaxy, we built a much deeper optical catalog of the field from Pan-STARRS1 (PS1). PS1 covers to entire sky north of -30 degrees in the grizy bands. For the following we used the r-band (6215 nm) which has a magnitude limit of 23.2 (Chambers and Pan-STARRS Team, 2018). We used Mikulski Archive for Space Telescopes (MAST) services for retriving survey data for PS1 through `mastcasjobs`[1] and the wider query library `psquery`.[2] We queried all Pan-STARRS1 sources with 5 or more detections within 30" of the radio source, and cut out point sources using a ps_score threshold of 0.83 as described in Tachibana and Miller (2018). We then use PATH to estimate chance of association between the radio source and all galaxies in the field.

PATH Priors

For our PATH priors we provide and exponential offset prior and a magnitude galaxy prior. These favour closely offset radio sources and brighter host galaxies. PATH additionally allows us to consider an unknown prior P(U) in the association. The unknown prior represents the probability that the host of the source is not within the PS1 catalog. Low values of P(U) will prevent PATH from associating a high probability to the only source in the field regardless of the association probability as described in Seebeck et al. (2021). To determine a value of P(U) we take an additional result from Seebeck et al. (2021) reproduced in (Figure 2.3).

In Seebeck et al. (2021) we simulated FRB populations with the aid of a recent semi-analytic galaxy formation model (L-galaxies; Henriques et al., 2015) applied to dark-matter halo catalogues from the Millennium simulation (Springel et al., 2005). Our technique was broadly similar to that used by Safarzadeh et al. (2020), who generated their own galaxy catalogues using semi-empirical relations between galaxy and halo properties. We then implemented two schemes to choose FRB host galaxies: one where the likelihood of a galaxy hosting an FRB is proportional to SFR, and one where the likelihood is proportional to M_*. We used a linear probability scale to randomly choose a fixed number of FRB host galaxies according to each scheme of weighting potential FRB hosts. We also split our simulated FRB host-galaxy catalogues into three redshift bins ($z < 0.5$, $0.5 \leq z \leq 2$, $z > 2$), to better understand the effects of cosmic evolution. Additionally we chose locations of

[1] `https://github.com/rlwastro/mastcasjobs`
[2] `https://github.com/realfastvla/psquery/`

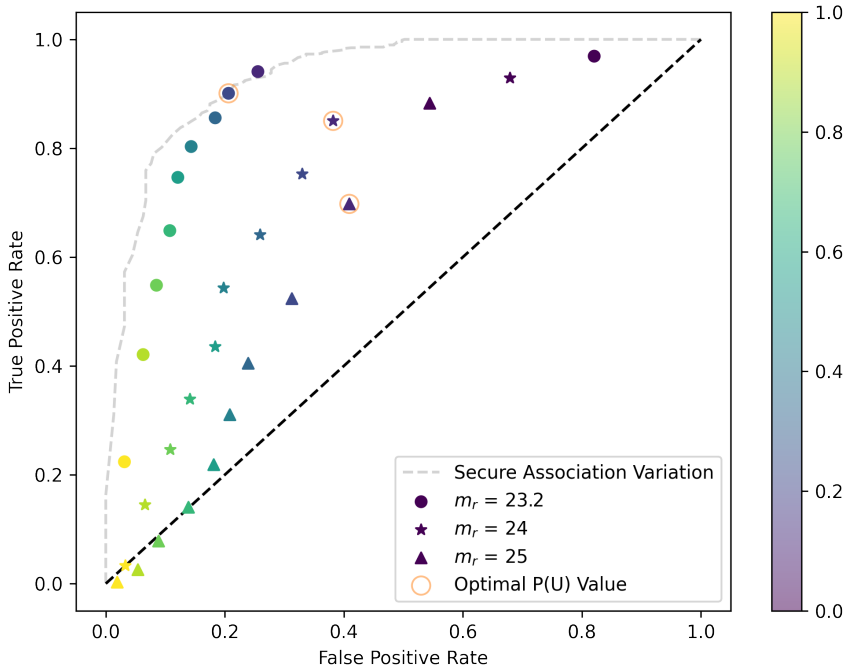

Figure 2.3: ROC curves indicating the effect of $P(U)$ and the magnitude limit of the optical survey on the TP and FP rates from PATH. All results were derived for 1,000 FRBs distributed according to SFR at $z < 0.5$. The symbols show results for different r-band magnitude cutoffs, as labelled, where $P(U)$ was varied between 0 and 0.9 according to the colour bar. Optimal values of $P(U)$ chosen according to a minimal distance to the point (0,1) (i.e., $FP = 0$, $TP = 1$) are indicated by orange circles. The grey dashed curve shows results for a variation in the secure association threshold between 0 and 1, with $P(U) = 0.2$ and a magnitude cutoff of 23.2. (Figure 6; Seebeck et al., 2021).

FRBs within the host galaxies by adopting a simple exponential model for the radial distributions of both stellar-mass and SFR distributions within galaxies (identical to Safarzadeh et al., 2020).

Relevant to this thesis are a series of simulated PATH associations of 1,000 $z < 0.5$ FRBs distributed among galaxies according to SFR, where we vary $P(U)$ between 0 and 0.9 in order to test for an optimal value. In these simulations we applied PATH to each of the FRBs and accepted associations that had a probability of 0.7 or greater. We call this cutoff the secure association cutoff. Then we calculate the true positive rate (TPR) and false positive rate (FPR), defined in nomenclature, for the sample to create an ROC curve. An ideal method for associations should have a

TPR = 1.0 and a FPR = 0.0: correctly identifying every FRB that has a host in the observed sample and not incorrectly associating those that do not.

This thesis will focus on the $m_r \leq 23.2$ magnitude simulations which predict and optimal P(U) = 0.2. In consideration of that value we will adopt a more conservative prior to account for possible differences in how our population of radio sources are distributed within galaxies, between galaxies, and other possible differences between the simulation and our catalog searches. Will continue by adopting a P(U) = 0.5. This decreases our TPR from 0.90 to 0.75 and decreases our FPR from 0.21 to 0.12. This causes us to not securely associate as many sources but be more confident in the sources we to associate. Additionally we raise to bar of our secure associations from 0.7 in the simulations to 0.9 to help raise our association confidence. Our final sample of accepted results will have a 217 candidates with at most 10 false positive sources predicted. But we expect less as we have chosen a more conservative secure association cutoff than the simulations.

Association Results

With the galaxy, offset, and unknown priors input into PATH algorithm we run associations for each of the 2767 candidates in our sample. This approach leverages the depth of the PS1 catalog and the rich information (esp distance) measured by GLADE+. Of our 2767 cross-matched sources after we apply our secure association cut of 0.90 we have 561 remaining source as seen in the orange distribution of Figure (Figure 2.2). This distribution still maintains an initial peak for nuclear sources but has a much smaller secondary rise at larger angular separations than the cross-matched sources. An example of a accepted association can be seen in in (Figure 2.4). Here we see the primary candidate 3 has a association probability of 0.958 while none of the other considered candidates have a probability ≥ 0.001. Due to the unknown prior, the remaining 0.042 of probability is attributed to the host being unseen. Additionally there is a fairly bright source close to the candidate which has been ruled out as a likely point source.

2.4 PS1-GLADE Reassociations

Our final step is to take those PATH chosen sources for each VLASS source and compare them to the original GLADE+ cross-matched galaxy. Our current sample contains any high probability association of a VLASS source to a PS1 counterpart but if that PS1 source is not the GLADE+ source then we should rule it out of our sample. We do this by accepting GLADE+ sources which are within 1" of the radius

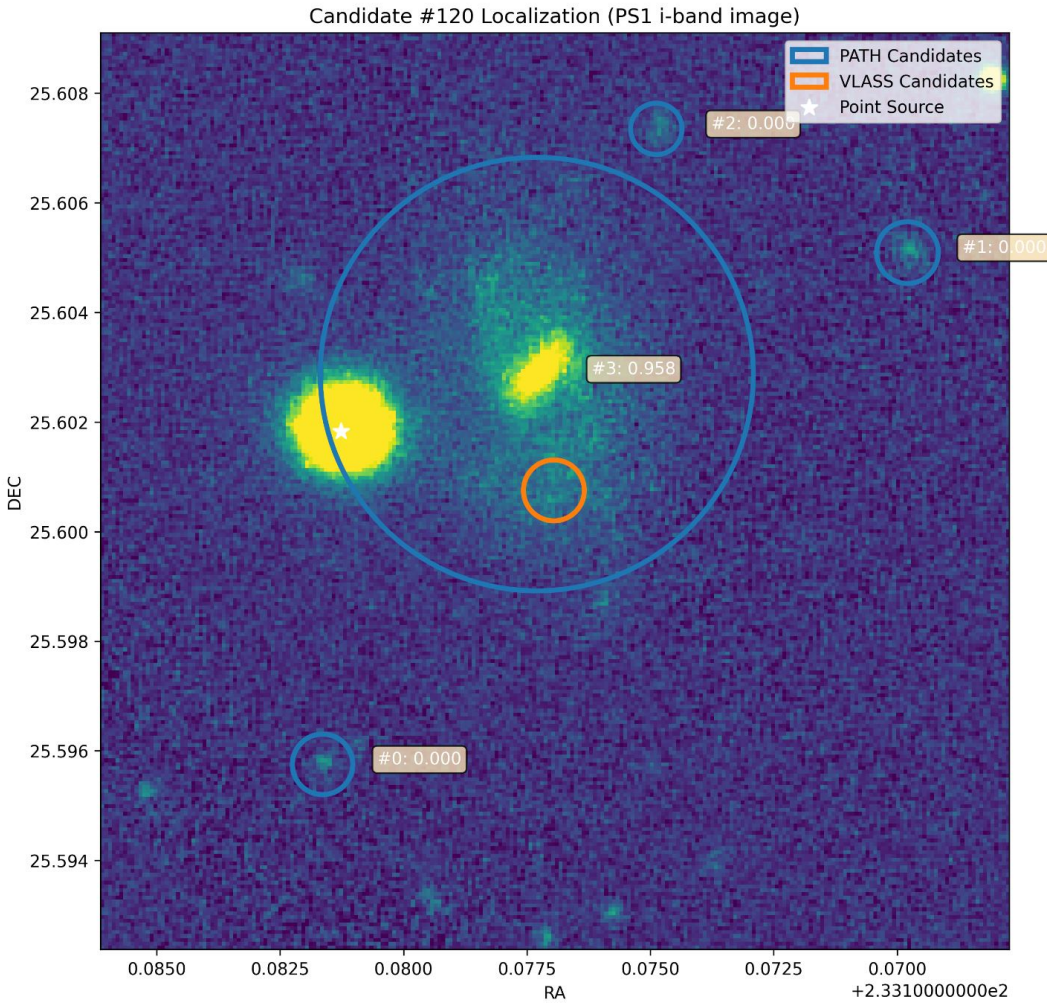

Figure 2.4: PS1 i-band image showing PATH association for candidate 120. The queried sources considered have blue circles and their association probabilities. Sources ruled out as point sources are marked with a white star. The VLASS uncertainty ellipse is shown in orange. The primary candidate has a association probability of 0.96

of the PATH source. Some misassociations can, and do, still result from this method: if the PS1 source has a large radius or if there are cluster of nearby sources around the radio source. Still, this gives us a sample of VLASS radio sources that we are reasonably confident are associated with dwarf galaxies from the GLADE+ catalog. Our final result includes 217 sources which can be seen in the green distribution in (Figure 2.2). The distribution still maintains a smaller but still present peak of nuclear sources. After a brief dip the distribution also shows a small peak at around 10" before falling again. This secondary rise is likely due to a population in galaxies

of larger angular size. This is confirmed through analysis of a histogram of physical offset (kpc) which does not show a high offset bump.

2.5 Initial Source List

Our result from this pipeline is a sample of 217 radio sources confidently associated with a GLADE+ dwarf galaxy. The method we have described has distinct advantages for discovering off-nuclear sources in large scale catalogs. Previous methods such as that seen in Reines, James Condon, et al. (2020) cross match a radio and optical catalog and then apply a cut at 5" not considering any further offset sources due to to probability of chance alignments. However our method allows us to systematically rule out chance alignment.

Figure 2.5 show the distributions of our sample of 217 sources. Radio luminsities follow a relatively log normal distribution around $10^{29} erg s^{-1} Hz^{-1}$ with a secondary peak at the large end $10^{31}\ erg\ s^{-1}\ Hz^{-1}$. This secondary peak is due to our high redshift sources. The sensitivity of VLASS causes only extremely bright sources to be seen at higher redshifts which causes a gap in detections in the middle. Due to our cut at $3 \times 10^7 M_\odot$, we have source hosts which are typically lower in magnitude and much lower masses in our sample compared to the original GLADE+ catalog. This also causes us to largely select low redshift galaxies.

A color magnitude diagram for the host galaxies of the 217 initial candidates is shown in Figure 2.6. This uses photometry from the g, r, and i PS1 bands for sources that had all 3. We see that most of our sources lie on in the blue SF main sequence, indicating a younger star forming galaxy sample. There are a sample of high magnitude, red galaxies which correspond to our high redshfit sample.

Possible issues such as incorrect PATH associations, incorrect GLADE+ realignment, and possible duplicates still remain in our catalog. Duplicates and realignment/association issues are fairly easy to resolve visually and due to our fairly low sample size this can be done manually. Additionally since our FPR is expected to be fairly low 0.12, PATH issues such as the circular shape assumption of galaxies, may be easy to spot visually. Generally our approach was to cast a fairly wide net with the initial catalog with the assumption that we can trim the catalog later on when it shrinks due to other analysis. The catalog will operate as a good starting point for further analysis. We will proceed with analysis of galaxy spectral energy distributions (SED) to refine our mass measurements, and get SFR, extinctions, and metallicities for our sources. These properties will help us further trim down our

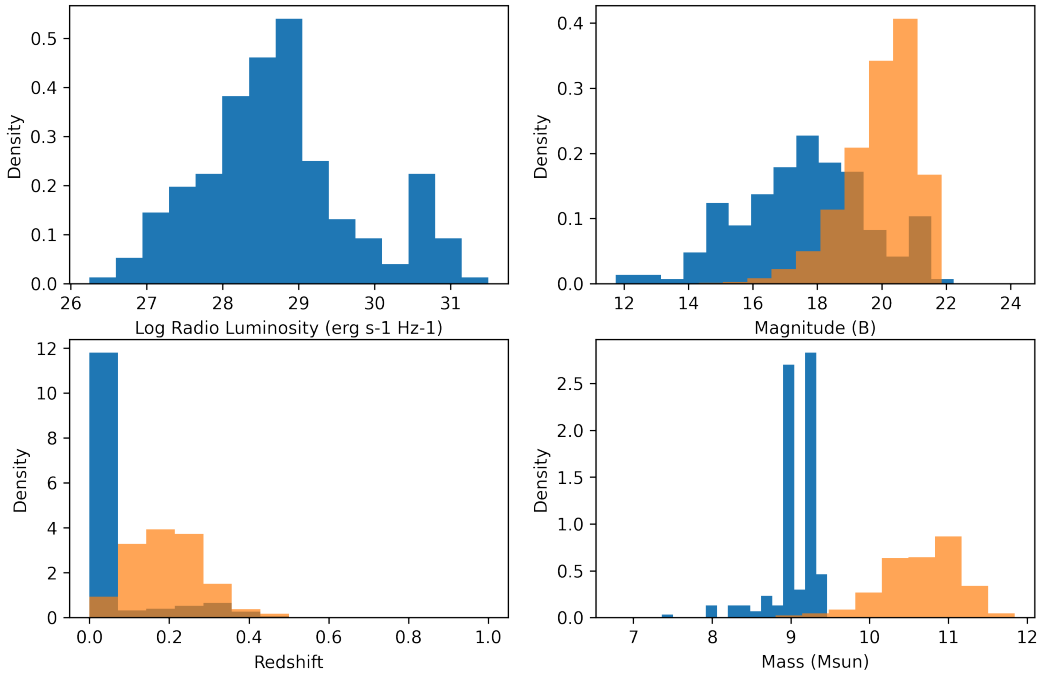

Figure 2.5: Histogram for different properties initial candidates (blue) and the GLADE+ catalog (orange). Distributions for L_{3GHz}, Magnitude (B), redshift, and Stellar Mass are included. Due to the size of GLADE+ a random sample of 10,000 sources is used for the histogram.

candidates as described in Section 2.7.

2.6 Spectral Energy Distributions

Querying Surveys

For each of our 217 sources we collected archival photometric observations with the intention of fitting spectral energy distributions (SEDs) to discern intrinsic properties like star formation rate and stellar mass. SED modelling to infer stellar properties requires 3 components: observations, a spectral model, and an analysis tool to help align the models to observations.

For the first component, our observations, we cast a wide net from the ultraviolet to the infrared surveying a few different catalogs, the completeness of our search can be seen in Table 2.1. Each of our sources has photometry in at least the r-band of PS1 (as required by PATH analysis), although most have photometry in all or most of the PS1 filters grizy. However due to issues with the redder bands of PS1 photometry we prefer the use of the DECam Legacy Survey (DECaLS; Dey et al., 2019) for our optical data. Out of our 217 sources 151 have data in DECaLS, for

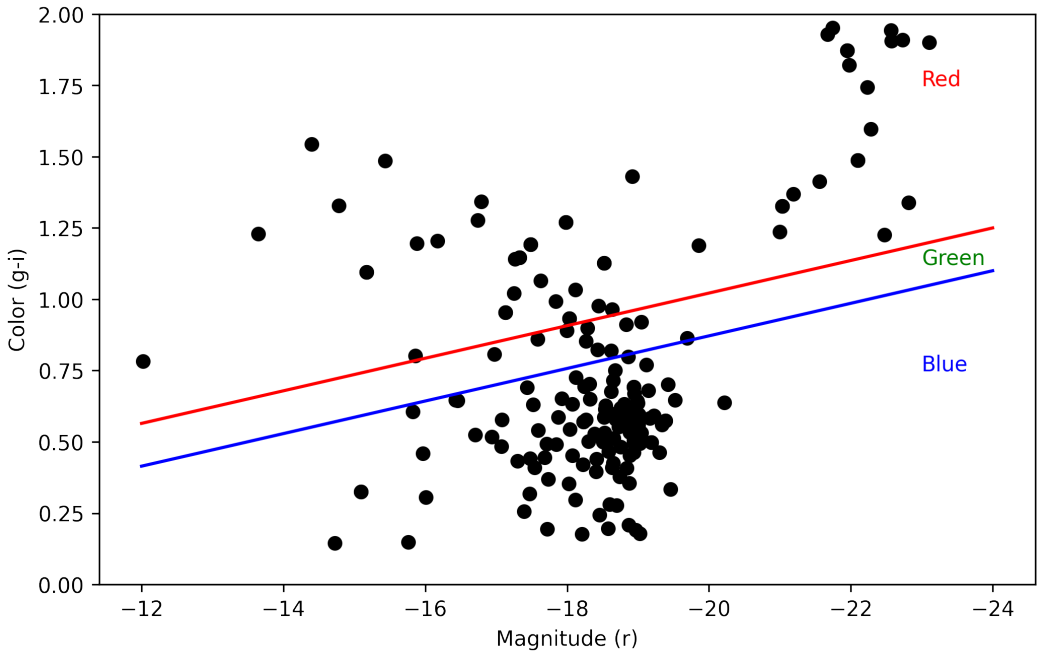

Figure 2.6: Color (g-i), magnitude (r) for the 217 initial PRS candidates. Photometry taken from the PS1 catalog, corrected for galactic extinction, and converted to absolute magnitudes using the GLADE+ redshfits. The red boundary line is given by g - i = 0.0571(M_r + 24) + 1.25, while the lower blue boundary line is parallel to the former with a 0.15 mag color offset from it (Papastergis et al., 2013). These lines separate the red sequence of galaxies from the green valley in the center, and the blue sequence on the bottom.

the remaining 66 sources we fall back onto PS1 for optical data. In the infrared we survey the ALLWISE data release (Cutri et al., 2021) from the Wide-field Infrared Survey Explorer (WISE; Wright et al., 2010). For SED analysis we only used the WISE W1 and W2 bands due to larger uncertainties in the W3 and W4 bands. 214 of our sources have data in the WISE W1 and W2 bands. We also surveyed the ultraviolet Galaxy Evolution Explorer (GALEX; Martin et al., 2005) survey in their FUV and NUV bands. 101 sources have data in the FUV and 147 in the NUV.

In order to avoid source confusion for these large queries we only accept the nearest source that is within the PS1 r-band Kron radius of the source, similar to our GLADE+ reassociations in Section 2.4. We again used `psquery` for all archival queries.

Survey	Filter	Number of Candidates
GALEX	FUV	101
GALEX	NUV	147
PS1	g	56
PS1	r	66
PS1	i	60
PS1	z	58
PS1	y	59
DECaLS	g	151
DECaLS	r	151
DECaLS	z	151
WISE	W1	214
WISE	W2	214

Table 2.1: Number of candidates with photometry in each photometric band queried for SED fitting. We queried GALEX, PS1, DECaLS, and WISE. Note that we first queries for DECaLS and if there was no data (66 source) then we used PS1 optical photometry.

SED Fitting

We used `prospector` (Johnson et al., 2021), a package for inference of stellar population properties with flexible models. `prospector` works as the third component of SED fitting allowing fitting of stellar population models to our photometric data. This uses either `emcee` (Foreman-Mackey et al., 2013) or a least-squares method. Due to the lack of reliable results of the least-squares method we use the Monte Carlo Chain Ensemble sampler textttemcee with with 100 (burnin) + 1000 steps for all of our sources. The second component, the models, are created with the Flexible Stellar Population Synthesis (`fsps`) code (Conroy, Gunn, and White, 2009). We choose a standard 'delay-tau' ($SFR \sim t_{age}\, e^{-t_{age}/\tau}$) parametric star formation history model and fixed the redshift at the reported GLADE+ values except for candidates 148 and 212 which we used their LRIS spectroscopic redshifts discussed in Section 4.2.

We applied a log-uniform prior in stellar mass from 10^8 – $10^{12} M_\odot$. This prior should account for galaxies as low mass as $10^7 M_\odot$ which is just below the GLADE+ minimum mass but there was an error in our code and the result is the $10^8 - 10^{12} M_\odot$ prior. Other priors included a top-hat prior on the internal dust extinction (A_V) of 0–1 magnitudes, a top-hat prior on the age of the stellar population of between 0.1–12.5 Gyr, a log-uniform prior on the star-formation timescale of between 0.1–1 Gyr, and a top-hat prior on the ratio of the metallicity to the solar metallicity ($logZ_{sol}$)

of between 2 and 0.2. We also make initial guesses of $M = 10^9 M_\odot$, A_V = 0.05, $logZ_{sol}$ = -0.63, t_{age} = 3 Gyr, and τ = 1 Gyr.

We check our querying and modelling with the source TC0221 (Somalwar et al., 2022). Our SED fit for this source is seen in Figure 2.7 and seems to give a very good fit, following our observational data well. From this fitting we report a $log(M_*/M_\odot) = 9.9^{-0.1}_{+0.1}$ which is relatively in line with the original result from Somalwar et al. (2022) of $log(M_*/M_\odot) = 10.15^{-0.07}_{+0.07}$. Additionally, there are very small discrepancies between our photometry and that of TC0221 but we explain these by our lack of account for host galaxy extinction. We do account for galactic extinction using the Schlegel, Finkbeiner, and Davis (SFD; 1998) dust extinction map, and the Fitzpatrick (1999) dust extinction function.

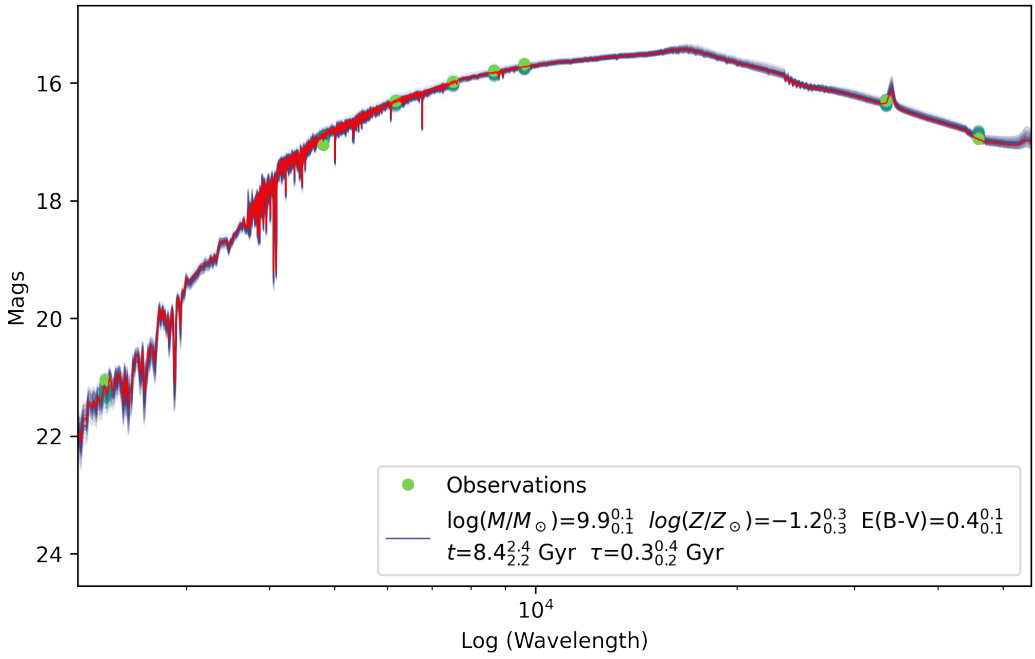

Figure 2.7: SED fitting for TC0221 using photometric data queried from GALEX, PS1, and ALLWISE. SED fitting done with the `prospector` stellar analysis code using a 'delay-tau' model. Fitting done with `emcee`, the maximum probability spectra is shown in red. Observed photometry shown is light green.

We initially attempted to query all of our sources with their corresponding PS1 photometry but noticed that some sources showed a 'dip' in the redder z and y bands. A dip at these wavelengths does not correspond to any similar trends in the galaxy models and thus could not be well fit by prospector. We did not find any distinct trends in these 'dip' sources that we felt explained this feature. We

likely attribute the error to issues with photometry calculation for extended sources. Although we did not find any trends related to size or blending with other objects. This issue with PS1 data is what motivated our use of DECaLS as our primary optical survey, as DECaLS photometry did not have this issue. To show this issue we take our VLBA sample from Section 3.3 and examine the photometry of each of the sources (Figure 2.8). Of the 11 VLBA sources 5 of them show a drop (Figure 2.8 Top) in the redder PS1 bands and 6 do not (Figure 2.8 Bottom). On the top plot with the 'drop' candidates we also have displayed the DECaLS data for the 2 sources (120 and 179) that have counterparts in that catalog. The improvement in overall shape from the PS1 to DECaLS data is clear, a standard model spectra can be seen in our example TC0221 (Figure 2.7). While 66 sources still use PS1 data we think that the primary use of DECaLS improves the reliability and consistency of our final data set.

SED Results

The results of our SED fitting for all 217 candidates can be seen in Figure 2.9. The middle row of Figure 2.11 shows two good fits from `prospector`, for sources 68 and 21, one with GALEX data and one without. In the mass plot we see a log-normal distribution centered around $10^9 M_\odot$, with a few candidates actually having masses over our original dwarf galaxy mass cutoff of $M_* \leq 10^9 M_\odot$. Additionally there is a build up at $10^8 M_\odot$ due to the mistake in our stellar mass prior. This would causes there to be less low-mass galaxies and for some SFRs to be lower than reported. Most of our fits show extremely low metallicities, and, based on the build up of values at $logZ_{sol}$ = -2.0, which is the low constraint of our prior, we infer that `prospector` would have fit even more low metallicity galaxies if the prior were altered. There is additionally a small build up at the other end of our metallicity prior. Our median galaxy mass is $8 \times 10^8 M_\odot$, and we have a median metallicity of $logZ_{sol}$ = -1.70. This places us 1.3 dex below the expected value from the mass-metallicity relation in the local universe (Curti et al., 2020). Our SFR distribution is fairly log-normal, centered around 0.12 $M_\odot yr^{-1}$ with a long tail for lower values. Showing a host galaxy population that is largely star forming dwarfs.

In Figure 2.10 we provide a goodness of fit for each of our candidates. For each photometric band used in the SED fitting we calculate a $\chi^2 = \frac{(obs-model)^2}{model}$ and take the average χ^2 for each candidate and multiply that by 1000 for ease of analysis. We place an cutoff at a χ^2 = 5 for 'good' fits. This was done by observing when the distribution in Figure 2.10 began to fall off and examining fits nearby χ^2 = 5,

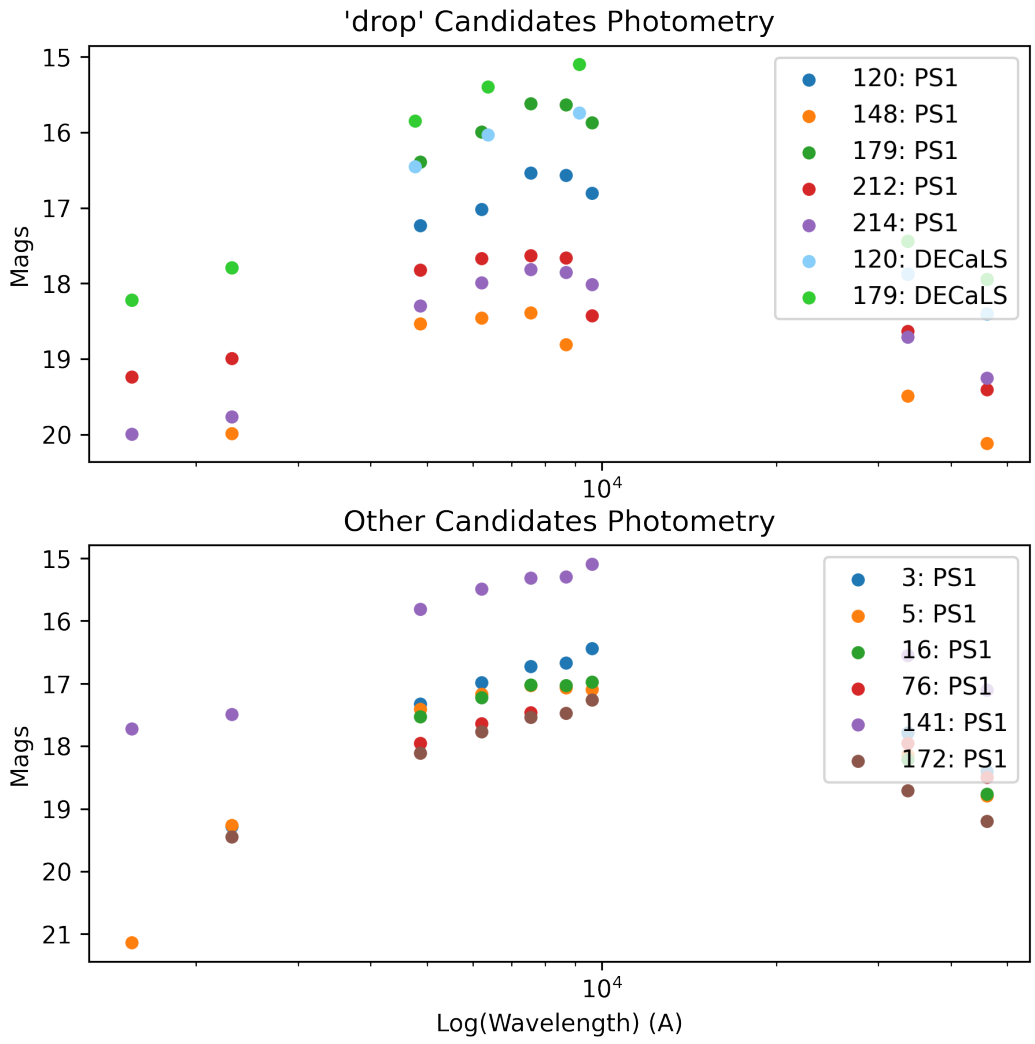

Figure 2.8: Top plot shows photometry for 'drop' candidates (120, 148, 179, 212, 214). The central points show optical photometry. The drop in the z and y bands can be seen for all of the candidates in the PS1 data. Two of the candidates (120, 179) appear in DECaLS and their photometry is also shown, with no drop in the z band. The PS1 photometry for the other candidates (3, 5, 16, 76, 141, 172) are shown in the bottom plot which display no drop in the z or y bands.

checking them by eye. 139 of our candidates have a $\chi^2 \leq 5$. The χ cutoff is not a hard line as their are still solid fits above the line and fits that have errors below it. Still it acts as a good measure for examining the general quality of SED fitting on our sample.

The largest category of high χ^2 fits have a distinct rise in their optical data which is unaccounted for in the model. We estimate nearly a third of our sources have some form of this error and half of those still show fairly reasonable fits just not below our

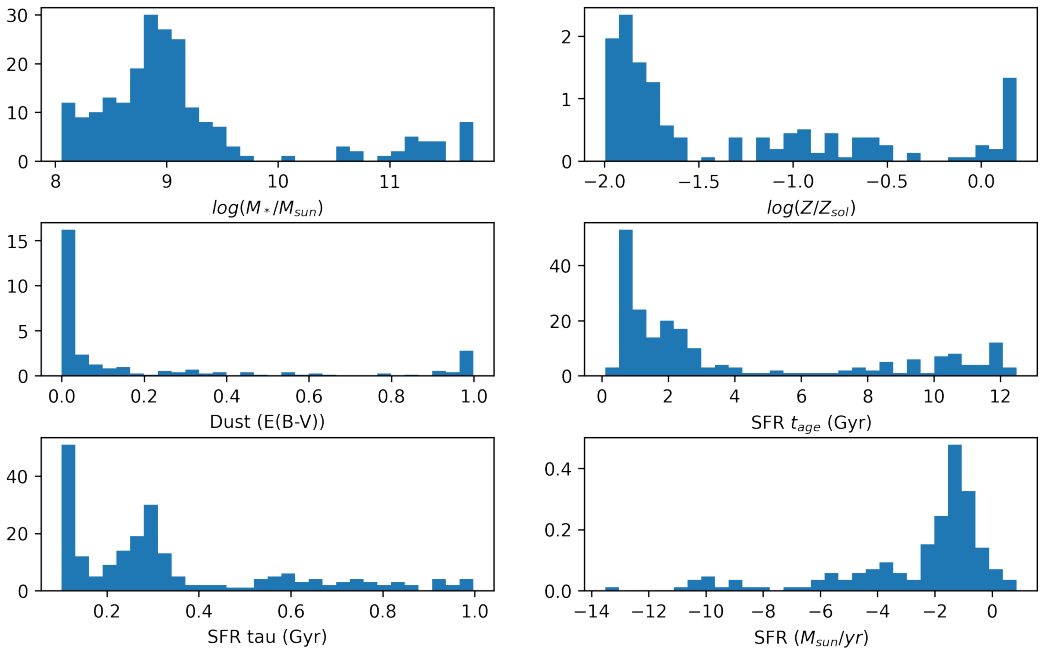

Figure 2.9: Histograms for each of the properties fit by `prospector` for the 217 initial candidates. The fit properties are stellar mass, metallicity, extinction, t_{age}, τ, and SFR.

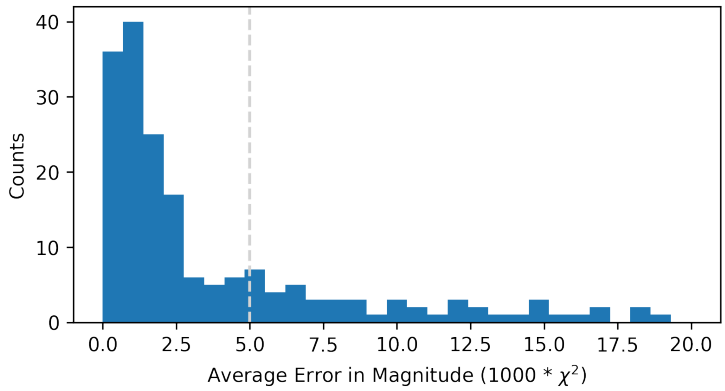

Figure 2.10: Histogram for the average χ^2 values/goodness of fits for the SED fitting procedure. We set a critical value of 5 for the χ^2 and consider values below this 'good' fits (gray dashed line). We established this value through analysis of the histogram drop off and visual analysis of the SED fits around the critical value.

χ^2 threshold. Two examples of this issue, candidates 68 and 21, are shown on the top row of Figure 2.11. These two sources have χ^2 values of 51 and 12 respectively, well above our 'good' fit threshold. These sources show a distinct 'jump' in their spectra at 4000 A in an attempt to fit the rise in optical data. This fit results in a

population of fairly young star forming sources.

We additionally note that some sources have photometry issues that cause them to be 'bad' fits. This is clear upon looking at the fit and seeing large variations in the data. Two examples of this, candidates 38 and 85, are shown on the bottom row of Figure 2.11. These two sources have χ^2 values of 191 and 329 respectively, well above our 'good' fit threshold. Although, candidate 38 does look to be a fairly reliable fit for all photometry except the NUV. One likely explanation is source misidentification between catalogs which would result in photometry from 2 different sources being used for SED fitting. Additionally there could be some survey level issue such as the previously discussed 'dip' PS1 sources, which still plague our SED fits. The SED process still needs refining for applications to larger candidate lists but with a fairly small sample size we can check sources individually as we narrow our candidate list. The process provided us valuable information in stellar masses and SFR for further analysis.

Luminosity from SFR

One of our main intentions from SED fitting was to obtain SFR for each of our candidates. This allows us to test the theory that the observed radio luminosity could be from ionized hydrogen in star forming regions. Or, that enough of it is that we cannot rule of other foregrounds such as SNe as an explanation for the emission. To do this we convert our radio flux density at 3 GHz to a flux at 1.4 GHz using Equation 2.1 (Equation 5; Delhaize et al., 2017). For α, Delhaize et al. (2017) recommend a value of -0.7 for redshift bins $z < 0.2$ which is appropriate for most of our sources. For this α they additionally predict a 1.4 GHz flux that is consistent with the 1.4 GHz limit only in 97% of cases.

$$L_{1.4GHz} = \frac{4\pi D_L^2}{(1+z)^{\alpha+1}} \left(\frac{1.4}{3}\right)^{\alpha} S_{3GHz} \tag{2.1}$$

Once we have a $L_{1.4GHz}$ for each source we then take the SFR from SED fitting and apply Equation 2.2 (Equation 17; Murphy et al., 2011) to get a $L_{1.4GHz}$ due to star formation. This equation is calibration based on the FIR–radio correlation (de Jong et al., 1985; Helou, Soifer, and Rowan-Robinson, 1985), which holds for our sample as the relation was established for globally integrated FIR and radio continuum galaxy properties.

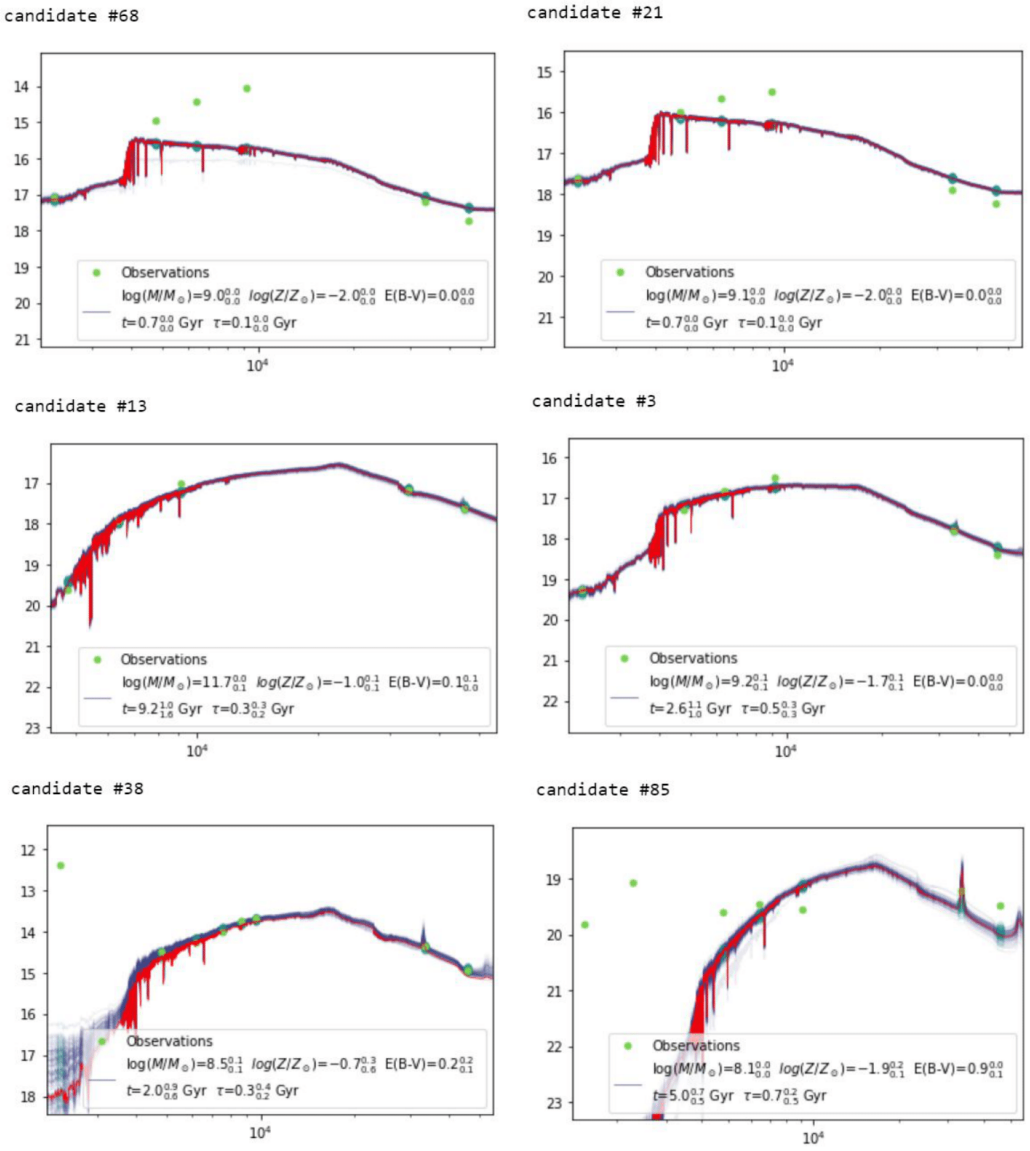

Figure 2.11: Example SED fits for 6 sources from our initial catalog, candidates 68, 21, 13, 3, 38, and 85. The units for the x-axis are a logarithmic wavelength scale in angstrom, the y-axis are magnitudes. The top row, candidates 68 and 21, show our category of 'rise' sources. Sources that are not fit well due to a large rise in thier optical data. This occurs at some level, not always as extreme, in 1/3 of our sources. The second row, candidates 13 and 3, show examples of good fits. The last row, candidates 38 and 85, show examples of candidates with photometry issues which have caused them to have bad fit qualities.

$$\left(\frac{SFR_{1.4GHz}}{M_\odot\ yr^{-1}}\right) = 6.35 \times 10^{-29} \left(\frac{L_{1.4GHz}}{erg\ s^{-1}\ Hz^{-1}}\right) \tag{2.2}$$

In the top panel of Figure 2.12 we can see our two distributions radio luminosity one from our VLASS sample and the other which has been converted from SFR as described above. The two distributions are shaped similarly with the SFR luminosities having a longer tail in lower luminosities. The key difference is that a VLASS sources typically has a luminosity of around 100 times greater than the luminosity from SFR. However the two distributions do overlap implying that some sources may have most of their VLASS luminosity explained by SFR. To explore that we look at the bottom panel of Figure 2.12. The contours on the plot use Equation 2.2 to show the amount of $L_{1.4GHz}$ that is explained by SFR for each source. We can see that a large majority (95%) of our sources have a $L_{1.4GHz}$ from SF that makes up less than 10% of the VLASS $L_{1.4GHz}$. 11 of our sources lie in the 10–50% range and no sources have higher than 50% with the largest being 41% for candidate 56. We do have an outlier which has more radio luminosity due to SF than from VLASS which not possible. Upon further inspection the SED for this source (2) only has 3 photometric measurements, and does only fits 2 of them well so we throw the SED of that result out.

We also included a number of sources from (Reines, James Condon, et al., 2020) where we have taken their flux density at 9 GHz and used Equation 2.1 to convert that to 1.4 GHz flux density. We then take the SFR from their Figure 3 and plot that here on Figure 2.12. We convert IDs 6, 10, 106, and 110ab which represent a wide range of luminosities, SFR, and AGN vs SF classifications. This notes a major discrepancy in between our results and that of (Reines, James Condon, et al., 2020) as roughly half of their sources have SFR which explain their radio luminosity while next to none of our sources do. The result of this plot shows that many of our sources do not have radio luminosities which can be explained by SFR and thus have high excess radio luminosities. If this radio excess exceeds $10^{29}\ erg\ s^{-1}\ Hz^{-1}$, then those sources still remain as possible PRS candidates. Thus the process of SED fitting has assisted us to rule out the astrophysical foreground of SFR as an explanation for the high radio luminosities of many of these sources.

2.7 Refining our Candidate List

Now we take the results from our SED fitting and initial associations to refine our sample down from 217 sources. In our search for PRS we are looking for sources that are:

- Offset from their hosts

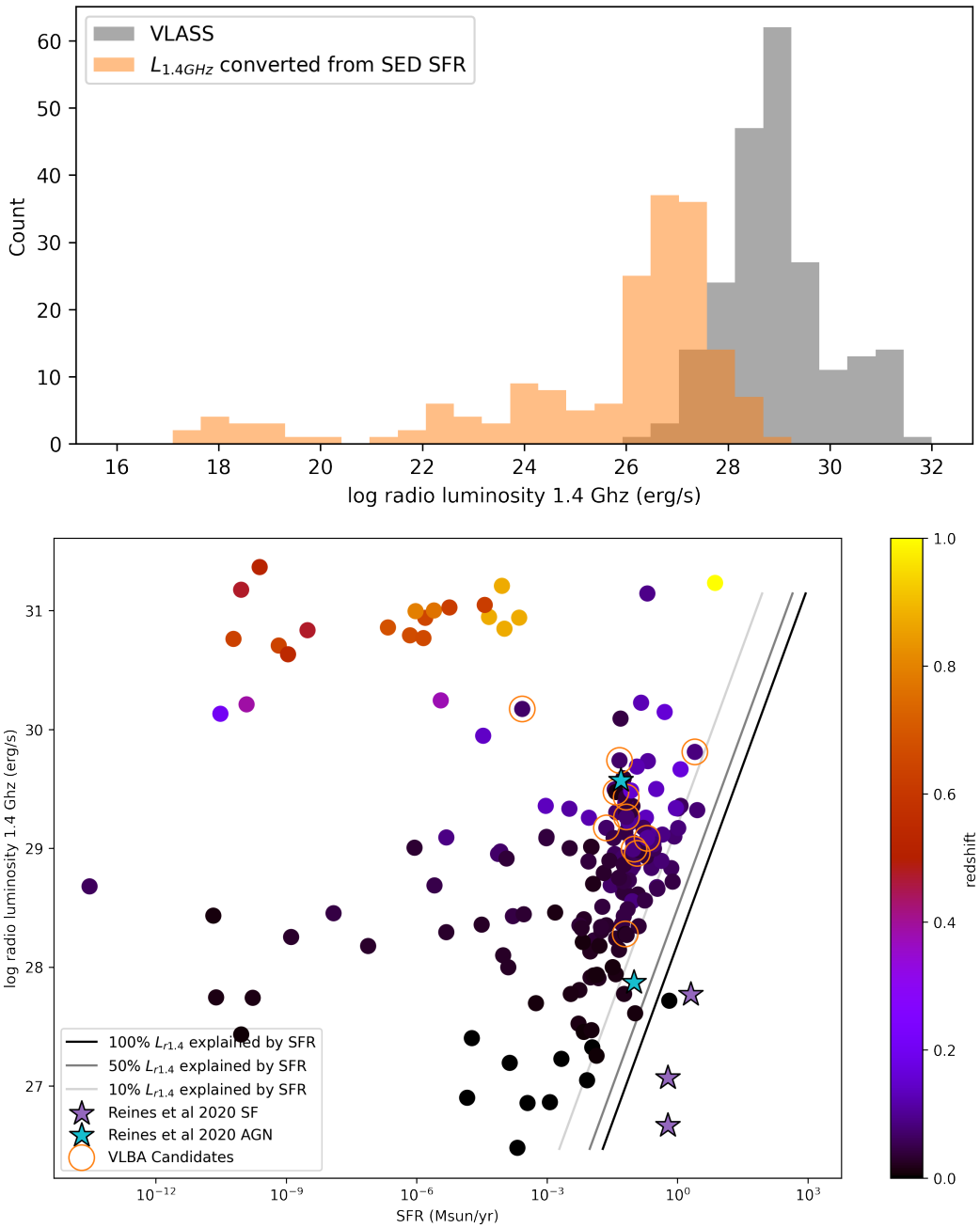

Figure 2.12: Top plot shows the histograms for the VLASS $L_{1.4GHz}$ and the $L_{1.4GHz}$ due to SFR converted from the SED fitting. Bottom plot shows VLASS $L_{1.4GHz}$ vs SFR $M_{\odot}yr^{-1}$. The scatter plot additionally has colorscale based on the GLADE+ redshifts of each of the sources. VLBA candidates, as discussed in Section **??**, have been outlined in orange. Contours based on Equation 2.1 are placed where SFR explains 10%, 50%, and 100% of the VLASS $L_{1.4GHz}$ are placed.

- Have a excess $L_{\nu} \geq 10^{29}\ erg\ s^{-1}\ Hz^{-1}$

- Have a high probability of association to their host galaxies

These features help us to eliminate a number of astonomical foregrounds and are in alignment with the properties of the two identified FRBs with PRS counterparts, 20121102A and 20190520B. High luminosity nuclear sources are very likely to be AGN and thus eliminating them lowers the likelihood of our candidates being AGN. AGN are not required to be at the centers of our galaxy and thus this cutoff does not eliminate their presence in our sample but it does lower it. Previous PRS have been identified as having radio luminosities around $L_\nu \geq 10^{29}\ erg\ s^{-1}\ Hz^{-1}$. Thus we are looking for sources with radio luminosities that exceed that value which cannot be explained by other common sources like star formation. Thus we take a measure of excess luminosity which is the radio luminoisty for each source which is not explained by luminosity from SFR which was derived in Section 2.6. Lastly we want to insure that our radio sources are associated with their host galaxies. This allows us to be confident in our galaxy properties which were vital in the previous two conditions we set on our PRS sample.

We first make a cut to only sources with excess $L_{1.4GHz} \geq 10^{29} erg\ s^{-1}\ Hz^{-1}$ which brings our sample down to 82 sources. We then look to the offsets of these sources. Figure 2.13 shows the offset of each source in arcseconds and kpc as compared to its excess luminosity. In the plot for kpc we can see a set of highly offset sources corresponding to high redshift sources. The remaining sample is mostly confined to less than 10 kpc. The plot additionally shows a lack of low luminosity high offset sources, but that does not play a factor for our analysis. In the arcsecond plot we can see two clear nuclear populations, one of low luminosity and high luminosity. The high luminosity sources are high redshift and thus their physical offset is estimated to be extremely large. Although due to their distance, errors in localization of the sources and their hosts can cause fairly large errors in physical distance. In order to account for these errors and eliminate nuclear sources we decide to take a cut of offset $\geq$ 2" for our sample. This brings our sample size down to 60. Lastly we make a final small cut on galaxy association probability taking VLASS sources which are 93% or more associated with their PS1 host, this leaves us with a sample of 32 sources.

We then provide a ranking of each of the sources by equally weighting and sorting for high log (excess L_r), high association probabilities, and low log M_*. This rank order provides just one way to look at the final source list, as other factors such as

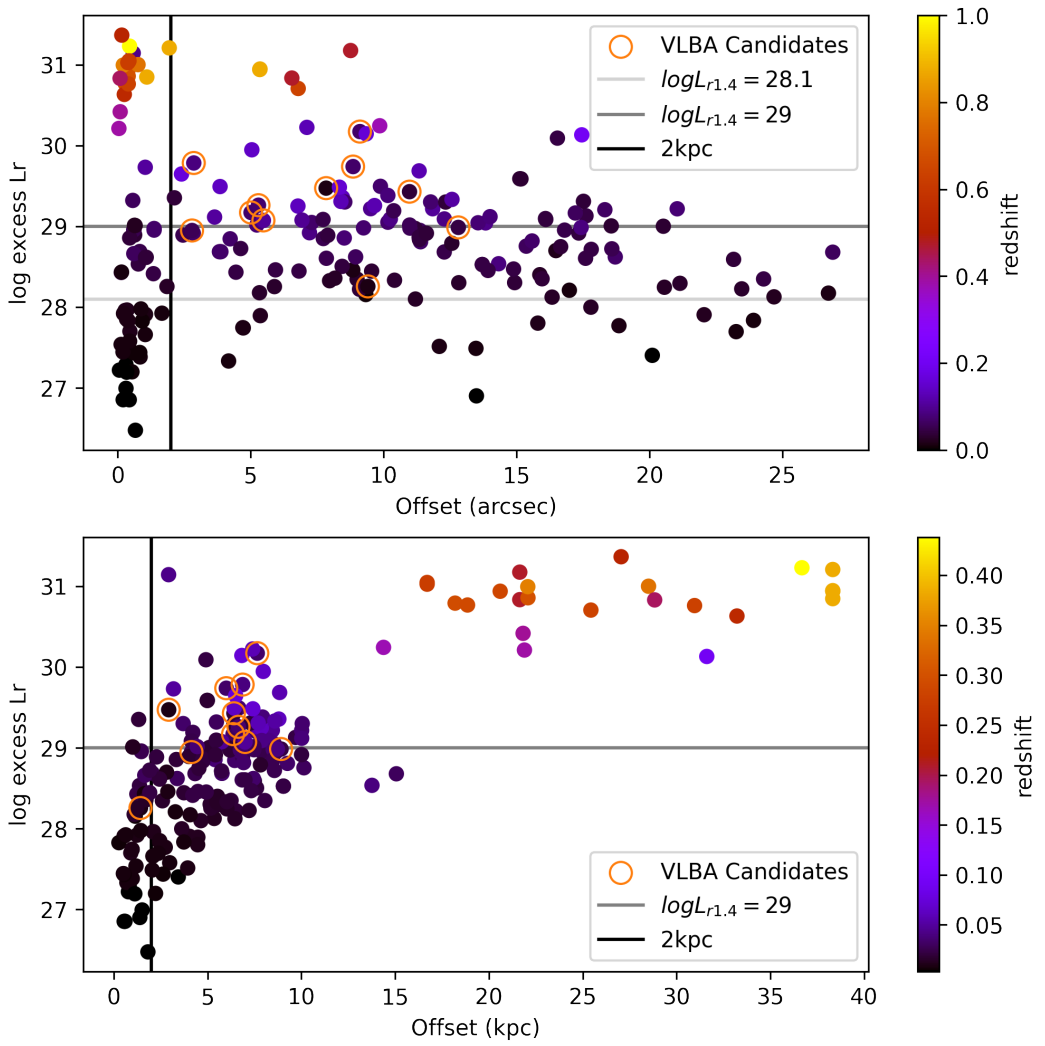

Figure 2.13: Excess radio luminosity vs offset of radio sources from the center of their galaxies. The top plot shows offset in arcseconds and the bottom plot shows offset in kpc which was calculated with the GLADE+ redshifts. VLBA candidates, as discussed in Section 3.3, are outlined in orange. A colorscale based on redshift is included in the plot. The PRS radio cutoff of 10^{29} erg s^{-1} Hz^{-1} is also included in the plot.

the quality of the SED fit, and PATH association as well as other properties should also be taken into consideration.

Our refined candidates list has 32 sources which based on the above considerations have a likelihood of being PRS. Next our job is to continue to eliminate more possible astrophysical foregrounds with follow up observations. These 32 sources provide an ideal starting point but the possibility that these sources are AGN or another source is still a possibility and needs to continue to be ruled out.

rank	ID	RA	DEC	Offset	Association	Redshift	Mass	SFR	$L_{1.4GHz}$
1	9	351.643	-20.884	2.135	0.989	0.019	8.153	0.092	29.352
2	212	136.027	53.054	2.863	0.973	0.039	8.627	2.509	29.784
3	213	59.840	-27.520	2.401	0.974	0.075	8.830	1.176	29.647
4	215	66.671	-14.555	5.047	0.964	0.066	9.256	0.000	29.947
5	5	149.018	16.239	9.112	0.951	0.033	9.114	0.000	30.173
6	108	5.525	-0.599	7.117	0.945	0.058	8.972	0.146	30.225
7	157	195.000	74.917	3.851	0.966	0.064	8.859	0.324	29.492
8	3	119.387	51.863	8.854	0.958	0.033	9.160	0.046	29.739
9	172	182.506	49.946	5.297	0.965	0.035	8.829	0.067	29.261
10	120	233.177	25.601	7.841	0.959	0.010	9.129	0.038	29.472
11	16	350.713	23.363	5.017	0.962	0.033	8.904	0.023	29.170
12	188	4.750	15.120	5.235	0.964	0.037	8.748	0.279	29.016
13	214	303.335	-14.745	5.483	0.964	0.049	8.943	0.199	29.073
14	141	180.673	56.380	10.977	0.953	0.019	9.108	0.066	29.429
15	94	170.168	31.599	6.551	0.937	0.210	11.163	0.000	30.835
16	55	227.896	0.784	9.883	0.939	0.035	8.931	0.036	29.495
17	142	180.675	56.381	12.335	0.948	0.019	9.121	0.066	29.300
18	41	172.805	24.925	8.543	0.932	0.033	8.361	0.039	29.301
19	121	233.175	25.600	11.771	0.945	0.034	9.131	1.020	29.301
20	58	174.871	-4.153	6.790	0.940	0.281	11.491	0.000	30.706
21	133	4.892	-2.894	17.518	0.937	0.019	8.788	0.083	29.309
22	184	125.502	57.324	10.982	0.946	0.028	8.816	0.279	29.015
23	100	33.558	-23.472	7.725	0.947	0.025	9.043	0.034	29.084
24	24	14.673	30.721	17.614	0.942	0.023	8.879	0.063	29.129
25	33	43.218	40.039	8.455	0.939	0.062	9.154	0.001	29.357
26	144	68.911	-6.619	8.398	0.931	0.058	8.672	0.919	29.308
27	174	9.389	-19.854	16.091	0.932	0.021	8.384	0.001	29.096
28	165	162.931	10.757	17.454	0.951	0.093	11.365	0.000	30.132
29	146	9.389	-19.854	16.101	0.932	0.021	8.386	0.001	29.085
30	75	229.499	7.101	7.297	0.950	0.033	9.403	0.000	29.047
31	62	179.305	-4.097	10.381	0.933	0.026	9.132	0.000	29.192
32	96	180.752	7.790	12.286	0.930	0.041	9.306	0.000	29.091

Table 2.2: Refined Candidate List for PRS. Created by cutting the initial 217 candidates by excess $L_\nu \geq 10^{29}\ erg\ s^{-1}\ Hz^{-1}$), offset > 2", and $P(O|x) \geq 0.93$. The table is in rank order based on equal weights of inverse log(mass), log(L_R), and association probabilty. The columns are as follows: 1-Rank, 2-Candidate ID number, 3-RA, 4-DEC, 5-Offset of radio source to PS1 source in arcseconds, 6-PATH association probability, 7-GLADE+ galaxy redshift, 8-Stellar Mass ($Log(M/M_\odot)$, 9-SFR ($M_\odot yr^{-1}$, 10-Excess radio luminosity from VLASS not explained by SFR ($ergs\ s^{-1}\ Hz^{-1}$).

Chapter 3

FOLLOW UP OBSERVATIONS

3.1 Overview

Due to the limited timescales of this thesis we have not been able to conduct extended follow up on these sources. Up this point we have been obtained optical spectra for two sources, and have proposed time for 11 sources during the 2022B observing semester of the VLBA. We intend obtain spectra and radio follow up with more of the refined sample (Table 2.2) in the future. Additionally we intend to follow up with radio SEDs. While VLBA is the most reliable method for confirming the size of emission for these sources radio SEDs can give us some information. We can look for a turnover at low frequencies. If that is seen, then the peak frequency can inform us about the density and size of the source. There are a large number of radio catalogs ASKAP RACS, LoTSS, VCSS, and the in development DSA-2000, which would be appropriate for this analysis.

3.2 LRIS Spectrum

We observed two PRS candidate galaxies (candidates 148 and 212) with the Keck Low Resolution Imaging Spectrometer (LRIS). The goal for these optical spectra is to improve redshift estimates and search for AGN ionization signatures, as has been used to identify AGN, even in dwarf galaxies (Molina et al., 2021).

We used 5 spectral lines to compute the redshifts of each of the galaxies. We report a redshift of 0.0389 ± .0004 for candidate 212 which is in agreement with the reported GLADE+ redshift of 0.0392. For candidate 148 we report a redshift of 0.0097 ± .0004 which is in extreme disagreement to the reported GLADE+ redshift of 0.0459. GLADE+ redshifts are photometrically calculated with an estimated mean relative error of 14% taken from the WISExSuperCOSMOS catalog. The major resulting effect of this redshift discrepancy is lowering the resultant radio luminosity from $2.52 \times 10^{29}\ erg\ s^{-1}\ Hz^{-1}$ to $1.11 \times 10^{28}\ erg\ s^{-1}\ Hz^{-1}$ below the tentative PRS threshold of $10^{29}\ erg\ s^{-1}\ Hz^{-1}$.

We explore many AGN indicator lines in both of these galaxies. (Molina et al., 2021) used the high ionization potential of the coronal line [Fe X]6374 as a AGN activity indicator. We found no presence of this line in either galaxy. We ad-

ditionally analyzed lines [OIII]5007, [NII]6583, [SII]6731,6716, [OI]6300 which are commonly used in Optical narrow emission-line diagnostic or commonly BPT diagrams (Mar Mezcua and Sánchez, 2020; Reines, James Condon, et al., 2020) to identify AGN based on the classification in Kewley et al. (2006). These diagrams compare line ratios for low-ionization lines commonly found in AGN to help show the presence of AGN, LINER, SEYFERT, and HII regions in objects. They compare the $[OIII]5007/H\beta$ ratio with other low ionization ratios. We find clear presence of the $[OIII]5007/H\beta$ ratio in both galaxies 212 and 148 with ratios of 3.36 and 3.45 respectively. However past this we find only evidence of $[SII]6731,6716/H\alpha$ in galaxy 212 with a ratio of 0.20. This places the candidate firmly in the HII region of the BPT diagram (Figure 1 Kewley et al., 2006). Spectra of these lines are shown in (Figure 3.1) for both candidates. The $[OI]/H\alpha$ lines are not shown in the plots as they were not present in either galaxy. The $[NII]/H\alpha$ ratio is shown in the figure to present an example of a non detection.

Through a scan of any emission lines present in these spectra we found a series of [OIII] lines but no other distinct emission lines. Also of note is the weak $H\alpha$ line of candidate 148 as compared to 212. This can be seen in Figure 3.1 and as the ratios to their comparably similar $H\beta$ are 1.28 for Cand 148 and 5.22 for Cand 212. Ultimately the spectra show no presence to confirm AGN activity in either galaxy due to lack of presence of common low and high ionization potential lines. Although this does not rule out AGN as the cause of radio emission in the galaxy it removes one possible detection method and PRS remain a possible solution to their identity.

3.3 VLBA Proposal

Sample Overview

We proposed observations during the 2022B semester of general observing for the Very Long Baseline Array (VLBA). The proposed observations were designed to eliminate alternative interpretations for the radio emission from the PRS candidates. The two major sources of astrophysical foregrounds are star-formation and AGN. The proposal was designated as C priority and will be scheduled as filler if there is available time during the 2022B observing semester.

During the creation of the proposal we had a limited sample of only 173 PRS candidates. The sample was identically created as the sample described in Chapter 2 but with a redshift limited GLADE+ catalog $z \leq 0.055$. Additionally at the time

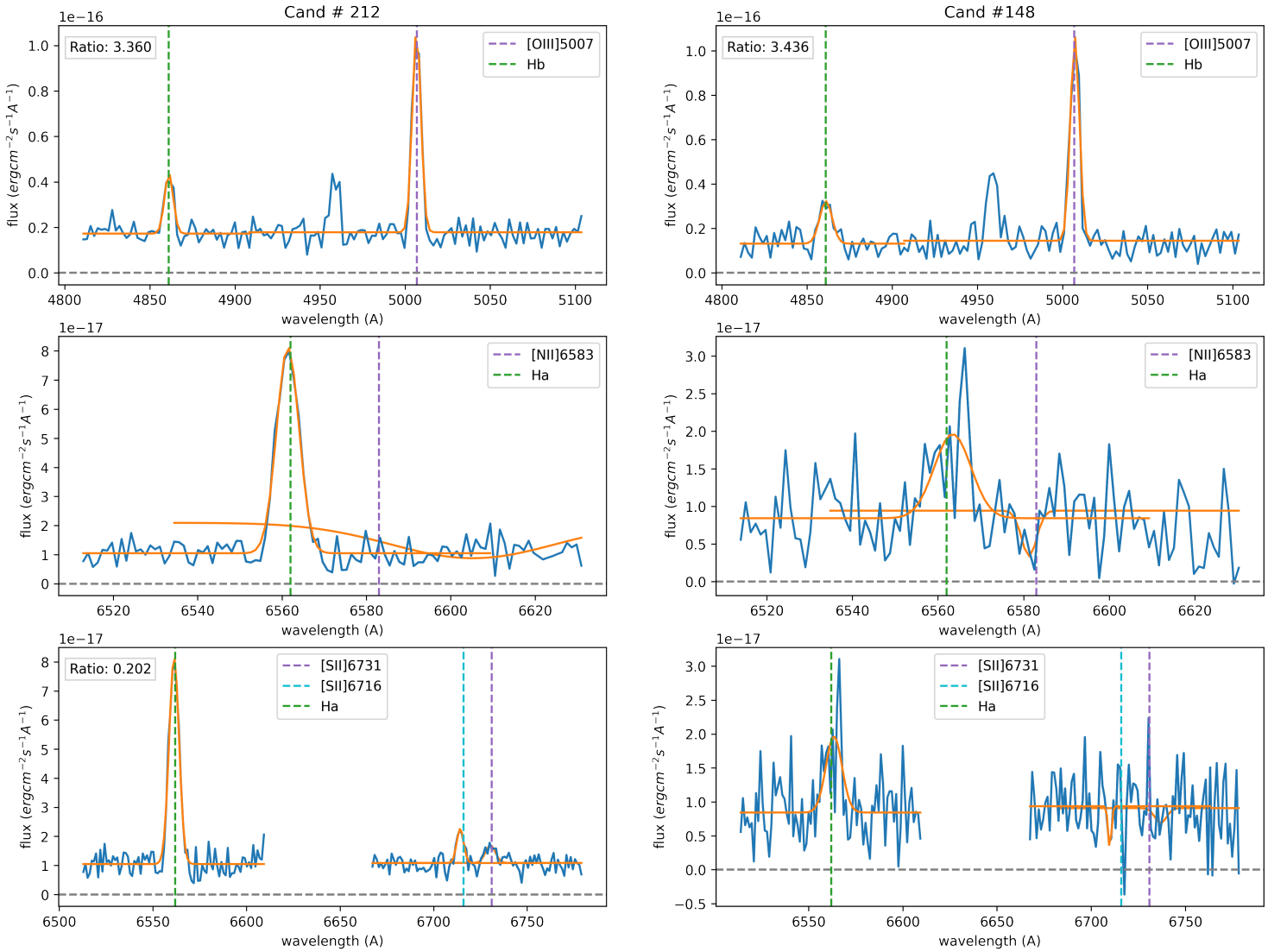

Figure 3.1: LRIS spectra of candidate 148 (right) and candidate 212 (left). The lines shown are common low ionization lines seen as common to AGN and used in BPT diagrams. Gaussian fits used to measure line equivalent widths for the strength ratios are shown in orange. If both lines are seen the ratio is listed in the upper left corner.

we did not have SED fitting for host galaxies and placed a cut of $5\times10^{28} erg\,s^{-1}\,Hz^{-1}$ on the sample instead of using excess luminosity. This left us with a sample of 16 PRS candidates with luminosity and offsets already inconsistent with expectations for supermassive black holes in galaxies of this mass ($M_{BH} < 2\times10^{5} M\odot$; Reines and Volonteri, 2015).

We further filtered this to a set of 11 by removing those with AGN signatures in

large spectroscopic catalogs or WISE colors (Secrest et al., 2015). Roughly half of the sample is spectroscopically identified as having no AGN signatures (Kovlakas et al., 2021). One of our target sample was also identified by Reines and Volonteri (2015, source ID 25) as a good example of an off-nuclear AGN in a galaxy with no spectroscopic signatures of AGN activity; this will be a valuable cross-check of the experimental design. None of these candidates are strong variables/transients between VLASS epoch 1 and 2, consistent with PRS models. Candidate 120 shown in Figure 2.4 is one of the proposed candidates. The candidates can be seen in Table 3.1 and images are shown in Figure 3.1. Note that candidate 148 was observed with LRIS spectra after our proposal which confirmed a much lower redshift that GLADE+ reported causing the radio luminosity to fall to $1.11 \times 10^{28}\ erg\ s^{-1}\ Hz^{-1}$ which is below our PRS threshold. This means candidate 148 is unlikley to be a PRS but is still included in this sample.

ID	RA	DEC	Offset	Association	Redshift	Mass	SFR	$L_{1.4GHz}$
3	119.387	51.863	8.854	0.958	0.033	9.160	0.046	29.739
5	149.018	16.239	9.112	0.951	0.033	9.114	0.000	30.173
16	350.713	23.363	5.017	0.962	0.033	8.904	0.023	29.170
76	135.804	48.404	2.797	0.975	0.028	8.565	0.118	28.948
120	233.177	25.601	7.841	0.959	0.010	9.129	1.034	29.449
141	180.673	56.380	10.977	0.953	0.019	9.108	0.066	29.429
148	272.465	53.450	9.411	0.955	0.010	8.540	0.063	28.255
172	182.506	49.946	5.297	0.965	0.035	8.829	0.067	29.261
179	324.784	4.248	12.812	0.952	0.023	8.969	0.100	28.986
212	136.027	53.054	2.863	0.973	0.039	8.627	2.509	29.784
214	303.335	-14.745	5.483	0.964	0.049	8.943	0.199	29.073

Table 3.1: Proposed candidates list for VLBA observations. List was created as described in Section 3.3. The columns are as follows: 1-Candidate ID number, 2-RA, 3-DEC, 4-Offset of radio source to PS1 source in arcseconds, 5-PATH association probability, 6-GLADE+ galaxy redshift, 7-Stellar Mass ($Log(M/M_{\odot})$, 8-SFR ($M_{\odot}yr^{-1}$, 9-Excess radio luminosity from VLASS not explained by SFR ($ergs\ s^{-1}\ Hz^{-1}$))

Proposed Observations

Star-formation activity is unlikely to produce radio luminosities seen for the PRS candidates. Three of the proposed sample have star-formation rate estimates that imply radio luminosities 10x lower than that observed by VLASS (James. Condon, Matthews, and Broderick, 2019). However, the L_R-SFR law has a large scatter, so a stronger test is required. Additionally from our SED fitting none of the sources had

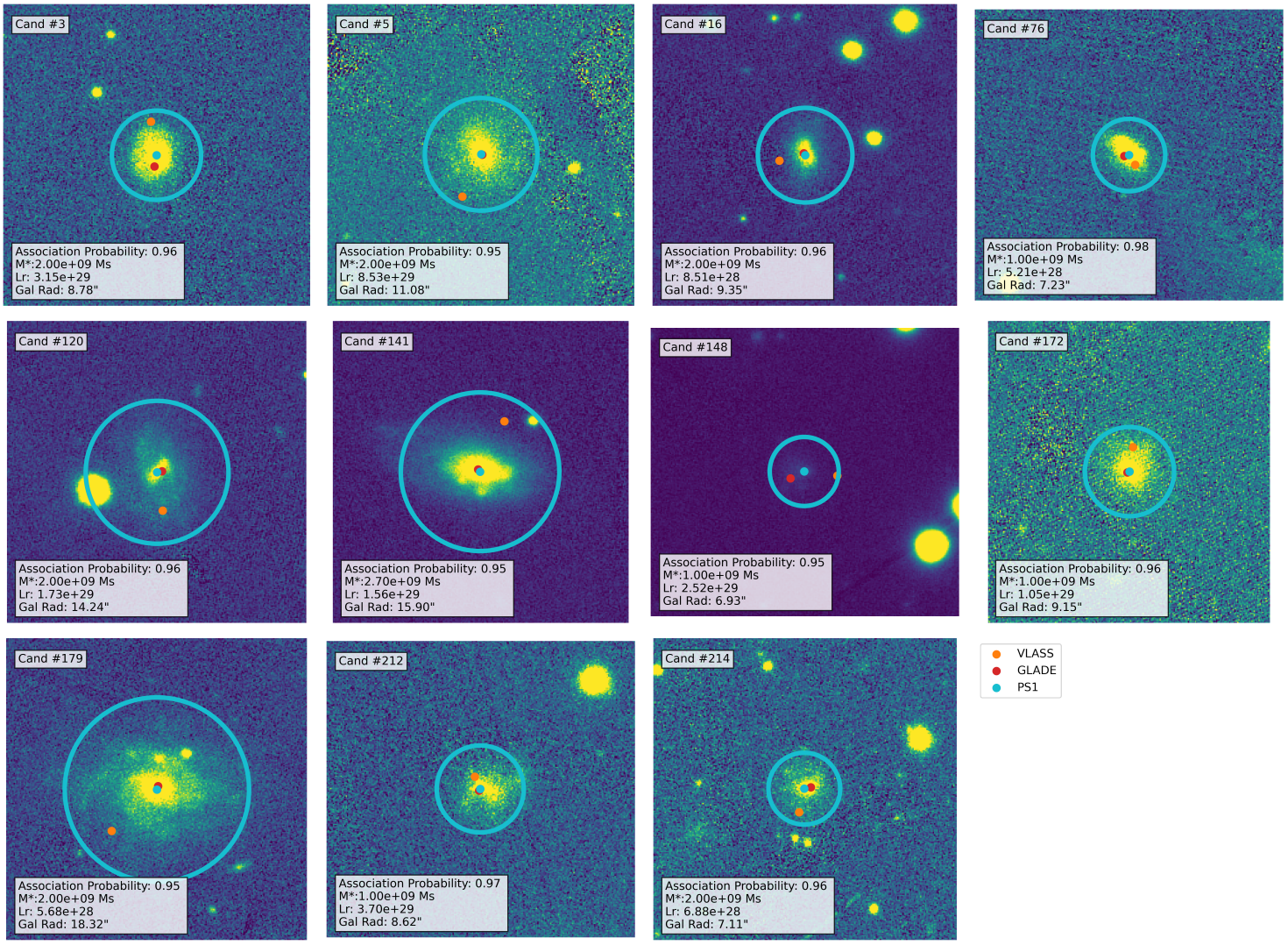

Figure 3.2: PS1 i-band images for each of the 11 VLBA candidates. The locations of the VLASS source (orange), GLADE+ source (red), and PS1 source (cyan) are shown for each image. The Kron radius of the chosen PS1 source is also shown. The association probability, stellar mass, VLASS radio luminosity, and galaxy radius are also shown.

a SFR that could account for more than 10% of the radio luminosity. Still we need to show that the radio emission is too compact to be consistent with star-formation activity (size < 1 kpc).

Our proposed VLBA imaging will resolve sources with a size of 1.4 mas and over-resolves on scales greater than roughly 20 mas. All sources are closer than $z = 0.05$ (~220 Mpc), where one milliarcsecond is equal to 1 parsec. The VLASS data have a physical resolution of roughly 1 kpc for our sample, so star-formation activity is

expected to be compact. The proposed observations will be able to resolve out kpc-scale emission associated with star-formation activity (as we have done for another PRS candidate; Vikram Ravi et al., 2021).

On parsec physical scales, it is also likely that compact jets from AGN can be identified. If they are AGN, then they are likely GHz-peaked Sources or Compact Symmetric Sources, the majority of which are larger than tens of parsecs (O'Dea, 1998). The precise position measured by the VLBA will also aid in ruling out AGN models. Any compact sources can be localized to an off-nuclear position and potentially associated to specific parts of the host galaxy. We can use the precise position to guide optical spectroscopy in a search for a (very rare) background galaxy.

The VLASS flux densities range from 1.2 to 31.9 mJy (median 5 mJy). We need a high-significance detection ($> 20\sigma$ for the weakest source), in order to interpret any non-detections. To reach this level, we proposed 10 minutes per target at 6 cm. If observed this program will allow us to further rule out astrophysical forgrounds such as AGN and star formation for this subset of our sample.

Chapter 4

CONCLUSION

4.1 Final Candidate Refinement

Our refined candidates sample Table 2.7 has 32 sources. In this section we will finalize that list with some small analysis and confirmation of our previous steps. First upon analysis of the images of all of the candidates we note that 120/121 and 141/142 radio sources from the same galaxy but do not seem to be duplicates. We also note that there was an error in the reassociation of the PS1 chosen source with the GLADE+ source for candidate 165. The GLADE+ source is not the PATH chosen source and thus falls below our acceptance threshold as the host galaxy so we remove 165 from our sample. We also remove 2 sources 9 and 188 which were identified in Section 3.3 as having WISE colors consistent with AGN activity. This leaves us with a final sample of 29 sources, which is in line with the estimate that motivated this thesis from Law, Connor, and K. Aggarwal (2021) that VLASS should detect between 4–830 PRS.

4.2 Concluding remarks

This thesis has outlined a novel procedure for large scale associations of radio source and optical galaxy catalogs for offset sources. This has allowed us to explore a new class of offset sources in search of the relatively unexplored phenomena of persistent radio sources. A summary of this process which narrowed down the VLASS catalog of 1,379,061 sources to one of 27 sources with reliable host galaxy information is described in Table 4.1. The largest cut comes from our cross matching of the GLADE+ catalog of 22.5 million sources–cut down to 390,533 dwarf galaxies–to the VLASS catalog. This along with our PATH association helped associate these sources to host galaxies and eliminate the possibility of them as background sources. Our additional analysis and cuts on luminosity, offset, and association probability help us lessen the probability of AGN, SNe, and SF regions as possible explanations for these incredible luminous sources. Additionally we outline spectral analysis for 2 sources which we plan to continue for the remaining sources to confirm redshifts and search for evidence of AGN activity. We also have proposed time on the VLBA in the hope of improving position and size measurements of these objects to hopefully confirm their compact nature similar to the two previously known PRS.

Number	Cutoff	Foreground Eliminated
1,379,061		
2,767	cross-matched within 30" of GLADE+	Background Sources
561	PATH probability ≥ 0.90	–
217	PATH to GLADE+ reassociation	–
82	excess $L_{1.4GHz} \geq 10^{29} erg\ s^{-1}\ Hz^{-1}$	SNe, SF regions
60	offset > 2"	AGN
32	PATH probability > 0.93	Background sources
29	WISE colors and visual analysis	AGN, errors in previous steps

Table 4.1: Summary of our process for creating a final list of 29 candidates for PRS from the 1,378,061 sources in the VLASS catalog. The columns are as follows: 1-Number of candidates remaining in the VLASS catalog, 2-The action applied to the previous sample which lowers the number candidates, 3-List of foregrounds that were target by the cut in column 2.

Ultimately this thesis presents a list of 27 candidates as persistent radio sources that need further follow up in order to continue to rule out astrophysical foregrounds and confirm them as PRS. If detected these sources would be the first PRS not discovered as a link to an FRB. Due to the extremely small existing sample size of PRS (2) this novel discovery would shed much insight onto these sources and their connections to FRBs. Additionally, given the extreme transient nature of FRBs the ability to research persistent sources connected to them is very insightful.

We would also like to touch on analysis being done on a very similar sample of sources described as 'wandering black holes' (Reines, James Condon, et al., 2020). These sources were gathered in a very similar method as this thesis but do not consider sources past 5". They do still observe a population of high excess luminosity sources offset from their host galaxies. Note none of the 39 sources identified in this paper are in our final sample. A new paper was recently released which reported on VLBI imaging of these sources (Sargent et al., 2022). Of their original sample of 13 sources they note the presence of compact sources consistent with accretion onto MBHs for 4 sources. However, as these sources are offset between 2"–5". The paper concludes that these sources are likely background AGN. However, due to their offset, compact nature, and high luminosity we propose that these sources are possibly linked with PRS.

BIBLIOGRAPHY

Aggarwal, Kshitij et al. (Apr. 2021). "Probabilistic Association of Transients to their Hosts (PATH)". In: 911.2, 95, p. 95. DOI: 10.3847/1538-4357/abe8d2. arXiv: 2102.10627 [astro-ph.HE].

Amiri, Mandana et al. (Dec. 2021). "The First CHIME/FRB Fast Radio Burst Catalog". In: 257.2, 59, p. 59. DOI: 10.3847/1538-4365/ac33ab. arXiv: 2106.04352 [astro-ph.HE].

Bannister, K. W. et al. (Aug. 2019). "A single fast radio burst localized to a massive galaxy at cosmological distance". In: *Science* 365.6453, pp. 565–570. DOI: 10.1126/science.aaw5903. arXiv: 1906.11476 [astro-ph.HE].

Bhandari, Shivani et al. (Feb. 2022a). "Characterizing the Fast Radio Burst Host Galaxy Population and its Connection to Transients in the Local and Extragalactic Universe". In: 163.2, 69, p. 69. DOI: 10.3847/1538-3881/ac3aec. arXiv: 2108.01282 [astro-ph.HE].

– (Feb. 2022b). "Characterizing the Fast Radio Burst Host Galaxy Population and its Connection to Transients in the Local and Extragalactic Universe". In: 163.2, 69, p. 69. DOI: 10.3847/1538-3881/ac3aec. arXiv: 2108.01282 [astro-ph.HE].

Bochenek, C. D. et al. (Nov. 2020). "A fast radio burst associated with a Galactic magnetar". In: 587.7832, pp. 59–62. DOI: 10.1038/s41586-020-2872-x. arXiv: 2005.10828 [astro-ph.HE].

Chambers, Kenneth and Pan-STARRS Team (Jan. 2018). "The Pan-STARRS1 Surveys". In: *American Astronomical Society Meeting Abstracts #231*. Vol. 231. American Astronomical Society Meeting Abstracts, 102.01, p. 102.01.

Chatterjee, S. et al. (Jan. 2017). "A direct localization of a fast radio burst and its host". In: 541.7635, pp. 58–61. DOI: 10.1038/nature20797. arXiv: 1701.01098 [astro-ph.HE].

Chen, Ge, Vikram Ravi, and Gregg W. Hallinan (Jan. 2022). "A comprehensive observational study of the FRB 121102 persistent radio source". In: *arXiv e-prints*, arXiv:2201.00999, arXiv:2201.00999. arXiv: 2201.00999 [astro-ph.HE].

Chibueze, James O. et al. (Dec. 2021). "A MeerKAT, e-MERLIN, H.E.S.S. and Swift search for persistent and transient emission associated with three localised FRBs". In: *arXiv e-prints*, arXiv:2201.00069, arXiv:2201.00069. arXiv: 2201.00069 [astro-ph.HE].

CHIME/FRB Collaboration, M. Amiri, et al. (Jan. 2019). "Observations of fast radio bursts at frequencies down to 400 megahertz". In: 566.7743, pp. 230–234. DOI: 10.1038/s41586-018-0867-7. arXiv: 1901.04524 [astro-ph.HE].

CHIME/FRB Collaboration, B. C. Andersen, et al. (Nov. 2019). "CHIME/FRB Discovery of Eight New Repeating Fast Radio Burst Sources". In: 885.1, L24, p. L24. DOI: 10.3847/2041-8213/ab4a80. arXiv: 1908.03507 [astro-ph.HE].

Condon, James., A. M. Matthews, and J. J. Broderick (Feb. 2019). "Radio Sources in the Nearby Universe". In: 872.2, 148, p. 148. DOI: 10.3847/1538-4357/ab0301. arXiv: 1901.10046 [astro-ph.GA].

Conroy, Charlie, James E. Gunn, and Martin White (July 2009). "The Propagation of Uncertainties in Stellar Population Synthesis Modeling. I. The Relevance of Uncertain Aspects of Stellar Evolution and the Initial Mass Function to the Derived Physical Properties of Galaxies". In: 699.1, pp. 486–506. DOI: 10.1088/0004-637X/699/1/486. arXiv: 0809.4261 [astro-ph].

Cordes, James M. and Shami Chatterjee (Aug. 2019). "Fast Radio Bursts: An Extragalactic Enigma". In: 57, pp. 417–465. DOI: 10.1146/annurev-astro-091918-104501. arXiv: 1906.05878 [astro-ph.HE].

Curti, Mirko et al. (Jan. 2020). "The mass-metallicity and the fundamental metallicity relation revisited on a fully T_e-based abundance scale for galaxies". In: 491.1, pp. 944–964. DOI: 10.1093/mnras/stz2910. arXiv: 1910.00597 [astro-ph.GA].

Cutri, R. M. et al. (Feb. 2021). "VizieR Online Data Catalog: AllWISE Data Release (Cutri+ 2013)". In: *VizieR Online Data Catalog*, II/328, pp. II/328.

Dálya, G. et al. (Oct. 2021). "GLADE+: An Extended Galaxy Catalogue for Multimessenger Searches with Advanced Gravitational-wave Detectors". In: *arXiv e-prints*, arXiv:2110.06184, arXiv:2110.06184. arXiv: 2110.06184 [astro-ph.CO].

de Jong, T. et al. (June 1985). "Radio continuum and far-infrared emission from spiral galaxies : a close correlation." In: 147, pp. L6–L9.

Delhaize, J. et al. (June 2017). "The VLA-COSMOS 3 GHz Large Project: The infrared-radio correlation of star-forming galaxies and AGN to $z \lesssim 6$". In: 602, A4, A4. DOI: 10.1051/0004-6361/201629430. arXiv: 1703.09723 [astro-ph.GA].

Dey, Arjun et al. (May 2019). "Overview of the DESI Legacy Imaging Surveys". In: 157.5, 168, p. 168. DOI: 10.3847/1538-3881/ab089d. arXiv: 1804.08657 [astro-ph.IM].

Dong, D. Z. et al. (Sept. 2021). "A transient radio source consistent with a merger-triggered core collapse supernova". In: *Science* 373.6559, pp. 1125–1129. DOI: 10.1126/science.abg6037. arXiv: 2109.01752 [astro-ph.HE].

Eftekhari, T. et al. (June 2020). "Wandering Massive Black Holes or Analogs of the First Repeating Fast Radio Burst?" In: 895.2, 98, p. 98. DOI: 10.3847/1538-4357/ab9015. arXiv: 2001.02688 [astro-ph.HE].

Eichler, David (Dec. 2017). "Nanolensed Fast Radio Bursts". In: 850.2, 159, p. 159. DOI: 10.3847/1538-4357/aa8b70. arXiv: 1711.04764 [astro-ph.HE].

Fitzpatrick, Edward L. (Jan. 1999). "Correcting for the Effects of Interstellar Extinction". In: 111.755, pp. 63–75. DOI: 10.1086/316293. arXiv: astro-ph/9809387 [astro-ph].

Foreman-Mackey, Daniel et al. (Mar. 2013). "emcee: The MCMC Hammer". In: 125.925, p. 306. DOI: 10.1086/670067. arXiv: 1202.3665 [astro-ph.IM].

Greene, Jenny E. and Luis C. Ho (Nov. 2007). "A New Sample of Low-Mass Black Holes in Active Galaxies". In: 670.1, pp. 92–104. DOI: 10.1086/522082. arXiv: 0707.2617 [astro-ph].

Heintz, Kasper E. et al. (Nov. 2020). "Host Galaxy Properties and Offset Distributions of Fast Radio Bursts: Implications for Their Progenitors". In: 903.2, 152, p. 152. DOI: 10.3847/1538-4357/abb6fb. arXiv: 2009.10747 [astro-ph.GA].

Helou, G., B. T. Soifer, and M. Rowan-Robinson (Nov. 1985). "Thermal infrared and nonthermal radio : remarkable correlation in disks of galaxies." In: 298, pp. L7–L11. DOI: 10.1086/184556.

Henriques, Bruno M. B. et al. (Aug. 2015). "Galaxy formation in the Planck cosmology - I. Matching the observed evolution of star formation rates, colours and stellar masses". In: 451.3, pp. 2663–2680. DOI: 10.1093/mnras/stv705. arXiv: 1410.0365 [astro-ph.GA].

Hilmarsson, G. H. et al. (Feb. 2021). "Rotation Measure Evolution of the Repeating Fast Radio Burst Source FRB 121102". In: 908.1, L10, p. L10. DOI: 10.3847/2041-8213/abdec0. arXiv: 2009.12135 [astro-ph.HE].

Johnson, Benjamin D. et al. (June 2021). "Stellar Population Inference with Prospector". In: 254.2, 22, p. 22. DOI: 10.3847/1538-4365/abef67. arXiv: 2012.01426 [astro-ph.GA].

Katz, J. I. (Feb. 2021). "The environment of FRB 121102 and possible relation to SGR/PSR J1745-2900". In: 501.1, pp. L76–L79. DOI: 10.1093/mnrasl/slaa202. arXiv: 2011.11666 [astro-ph.HE].

Kewley, Lisa J. et al. (Nov. 2006). "The host galaxies and classification of active galactic nuclei". In: 372.3, pp. 961–976. DOI: 10.1111/j.1365-2966.2006.10859.x. arXiv: astro-ph/0605681 [astro-ph].

Kirsten, F. et al. (May 2021). "A repeating fast radio burst source in a globular cluster". In: *arXiv e-prints*, arXiv:2105.11445, arXiv:2105.11445. arXiv: 2105.11445 [astro-ph.HE].

Kocz, J. et al. (Oct. 2019). "DSA-10: a prototype array for localizing fast radio bursts". In: 489.1, pp. 919–927. DOI: 10.1093/mnras/stz2219. arXiv: 1906.08699 [astro-ph.IM].

Kovlakas, K. et al. (Sept. 2021). "The Heraklion Extragalactic Catalogue (HECATE): a value-added galaxy catalogue for multimessenger astrophysics". In: 506.2, pp. 1896–1915. DOI: 10.1093/mnras/stab1799. arXiv: 2106.12101 [astro-ph.GA].

Law, C. J., G. C. Bower, et al. (May 2018). "realfast: Real-time, Commensal Fast Transient Surveys with the Very Large Array". In: 236.1, 8, p. 8. DOI: 10.3847/1538-4365/aab77b. arXiv: 1802.03084 [astro-ph.IM].

Law, C. J., L. Connor, and K. Aggarwal (Oct. 2021). "On the Fast Radio Burst and Persistent Radio Source Populations". In: *arXiv e-prints*, arXiv:2110.15323, arXiv:2110.15323. arXiv: 2110.15323 [astro-ph.HE].

Lorimer, D. R. et al. (Nov. 2007). "A Bright Millisecond Radio Burst of Extragalactic Origin". In: *Science* 318.5851, p. 777. DOI: 10.1126/science.1147532. arXiv: 0709.4301 [astro-ph].

Macquart, Jean-Pierre, M. Bailes, et al. (June 2010). "The Commensal Real-Time ASKAP Fast-Transients (CRAFT) Survey". In: 27.3, pp. 272–282. DOI: 10.1071/AS09082. arXiv: 1001.2958 [astro-ph.HE].

Macquart, Jean-Pierre, J. X. Prochaska, et al. (May 2020). "A census of baryons in the Universe from localized fast radio bursts". In: 581.7809, pp. 391–395. DOI: 10.1038/s41586-020-2300-2. arXiv: 2005.13161 [astro-ph.CO].

Mannings, Alexandra G. et al. (Aug. 2021). "A High-resolution View of Fast Radio Burst Host Environments". In: 917.2, 75, p. 75. DOI: 10.3847/1538-4357/abff56. arXiv: 2012.11617 [astro-ph.GA].

Marcote, B., K. Nimmo, et al. (Jan. 2020). "A repeating fast radio burst source localized to a nearby spiral galaxy". In: 577.7789, pp. 190–194. DOI: 10.1038/s41586-019-1866-z. arXiv: 2001.02222 [astro-ph.HE].

Marcote, B., Z. Paragi, et al. (Jan. 2017). "The Repeating Fast Radio Burst FRB 121102 as Seen on Milliarcsecond Angular Scales". In: 834.2, L8, p. L8. DOI: 10.3847/2041-8213/834/2/L8. arXiv: 1701.01099 [astro-ph.HE].

Margalit, Ben and Brian D. Metzger (Nov. 2018). "A Concordance Picture of FRB 121102 as a Flaring Magnetar Embedded in a Magnetized Ion-Electron Wind Nebula". In: 868.1, L4, p. L4. DOI: 10.3847/2041-8213/aaedad. arXiv: 1808.09969 [astro-ph.HE].

Martin, D. Christopher et al. (Jan. 2005). "The Galaxy Evolution Explorer: A Space Ultraviolet Survey Mission". In: 619.1, pp. L1–L6. DOI: 10.1086/426387. arXiv: astro-ph/0411302 [astro-ph].

Mezcua, M., H. Suh, and F. Civano (Sept. 2019). "Radio jets from AGNs in dwarf galaxies in the COSMOS survey: mechanical feedback out to redshift ∼3.4". In: 488.1, pp. 685–695. DOI: 10.1093/mnras/stz1760. arXiv: 1906.10713 [astro-ph.GA].

Mezcua, Mar and Helena Domı nguez Sánchez (July 2020). "Hidden AGNs in Dwarf Galaxies Revealed by MaNGA: Light Echoes, Off-nuclear Wanderers, and a New Broad-line AGN". In: *The Astrophysical Journal* 898.2, p. L30. DOI: 10.3847/2041-8213/aba199. URL: https://doi.org/10.3847%2F2041-8213%2Faba199.

Michilli, D. et al. (Jan. 2018). "An extreme magneto-ionic environment associated with the fast radio burst source FRB 121102". In: 553.7687, pp. 182–185. DOI: 10.1038/nature25149. arXiv: 1801.03965 [astro-ph.HE].

Molina, Mallory et al. (Dec. 2021). "A Sample of Massive Black Holes in Dwarf Galaxies Detected via [Fe X] Coronal Line Emission: Active Galactic Nuclei and/or Tidal Disruption Events". In: 922.2, 155, p. 155. DOI: 10.3847/1538-4357/ac1ffa. arXiv: 2108.09307 [astro-ph.GA].

Murase, Kohta, Kazumi Kashiyama, and Peter Mészáros (Sept. 2016). "A burst in a wind bubble and the impact on baryonic ejecta: high-energy gamma-ray flashes and afterglows from fast radio bursts and pulsar-driven supernova remnants". In: 461.2, pp. 1498–1511. DOI: 10.1093/mnras/stw1328. arXiv: 1603.08875 [astro-ph.HE].

Murphy, E. J. et al. (Aug. 2011). "Calibrating Extinction-free Star Formation Rate Diagnostics with 33 GHz Free-free Emission in NGC 6946". In: 737.2, 67, p. 67. DOI: 10.1088/0004-637X/737/2/67. arXiv: 1105.4877 [astro-ph.CO].

Niu, C. -H. et al. (Oct. 2021). "A repeating FRB in a dense environment with a compact persistent radio source". In: *arXiv e-prints*, arXiv:2110.07418, arXiv:2110.07418. arXiv: 2110.07418 [astro-ph.HE].

O'Dea, Christopher P. (May 1998). "The Compact Steep-Spectrum and Gigahertz Peaked-Spectrum Radio Sources". In: 110.747, pp. 493–532. DOI: 10.1086/316162.

Papastergis, Emmanouil et al. (Oct. 2013). "The Clustering of ALFALFA Galaxies: Dependence on H I Mass, Relationship with Optical Samples, and Clues of Host Halo Properties". In: 776.1, 43, p. 43. DOI: 10.1088/0004-637X/776/1/43. arXiv: 1308.2661 [astro-ph.CO].

Petroff, E., J. W. T. Hessels, and D. R. Lorimer (May 2019). "Fast radio bursts". In: 27.1, 4, p. 4. DOI: 10.1007/s00159-019-0116-6. arXiv: 1904.07947 [astro-ph.HE].

Pleunis, Ziggy et al. (Dec. 2021). "Fast Radio Burst Morphology in the First CHIME/FRB Catalog". In: 923.1, 1, p. 1. DOI: 10.3847/1538-4357/ac33ac. arXiv: 2106.04356 [astro-ph.HE].

Rajwade, Kaustubh et al. (Mar. 2021). "MeerTRAP in the era of multi-messenger astrophysics". In: *arXiv e-prints*, arXiv:2103.08410, arXiv:2103.08410. arXiv: 2103.08410 [astro-ph.IM].

Ravi, V. et al. (Aug. 2019). "A fast radio burst localized to a massive galaxy". In: 572.7769, pp. 352–354. DOI: 10.1038/s41586-019-1389-7. arXiv: 1907.01542 [astro-ph.HE].

Ravi, Vikram (July 2019). "The prevalence of repeating fast radio bursts". In: *Nature Astronomy* 3, pp. 928–931. DOI: 10.1038/s41550-019-0831-y. arXiv: 1907.06619 [astro-ph.HE].

Ravi, Vikram et al. (June 2021). "The host galaxy and persistent radio counterpart of FRB 20201124A". In: *arXiv e-prints*, arXiv:2106.09710, arXiv:2106.09710. arXiv: 2106.09710 [astro-ph.HE].

Reines, Amy E., James Condon, et al. (Jan. 2020). "A New Sample of (Wandering) Massive Black Holes in Dwarf Galaxies from High-resolution Radio Observations". In: 888.1, 36, p. 36. DOI: 10.3847/1538-4357/ab4999. arXiv: 1909.04670 [astro-ph.GA].

Reines, Amy E. and Marta Volonteri (Nov. 2015). "Relations between Central Black Hole Mass and Total Galaxy Stellar Mass in the Local Universe". In: 813.2, 82, p. 82. DOI: 10.1088/0004-637X/813/2/82. arXiv: 1508.06274 [astro-ph.GA].

Safarzadeh, Mohammadtaher et al. (Dec. 2020). "Confronting the Magnetar Interpretation of Fast Radio Bursts through Their Host Galaxy Demographics". In: 905.2, L30, p. L30. DOI: 10.3847/2041-8213/abd03e. arXiv: 2009.11735 [astro-ph.HE].

Sargent, Andrew J. et al. (May 2022). "Wandering Black Hole Candidates in Dwarf Galaxies at VLBI Resolution". In: *arXiv e-prints*, arXiv:2205.16006, arXiv:2205.16006. arXiv: 2205.16006 [astro-ph.GA].

Schlegel, David J., Douglas P. Finkbeiner, and Marc Davis (June 1998). "Maps of Dust Infrared Emission for Use in Estimation of Reddening and Cosmic Microwave Background Radiation Foregrounds". In: 500.2, pp. 525–553. DOI: 10.1086/305772. arXiv: astro-ph/9710327 [astro-ph].

Secrest, N. J. et al. (Nov. 2015). "Identification of 1.4 Million Active Galactic Nuclei in the Mid-Infrared using WISE Data". In: 221.1, 12, p. 12. DOI: 10.1088/0067-0049/221/1/12. arXiv: 1509.07289 [astro-ph.GA].

Seebeck, Jerome et al. (Dec. 2021). "The Effects of Selection Biases on the Analysis of Localised Fast Radio Bursts". In: *arXiv e-prints*, arXiv:2112.07639, arXiv:2112.07639. arXiv: 2112.07639 [astro-ph.HE].

Somalwar, Jean J. et al. (Apr. 2022). "The Nascent Milliquasar VT J154843.06+220812.6: Tidal Disruption Event or Extreme Accretion State Change?" In: 929.2, 184, p. 184. DOI: 10.3847/1538-4357/ac5e29. arXiv: 2108.12431 [astro-ph.HE].

Spitler, L. G. et al. (Mar. 2016). "A repeating fast radio burst". In: 531.7593, pp. 202–205. DOI: 10.1038/nature17168. arXiv: 1603.00581 [astro-ph.HE].

Springel, Volker et al. (June 2005). "Simulations of the formation, evolution and clustering of galaxies and quasars". In: 435.7042, pp. 629–636. DOI: 10.1038/nature03597. arXiv: astro-ph/0504097 [astro-ph].

Tachibana, Yutaro and A. A. Miller (Dec. 2018). "A Morphological Classification Model to Identify Unresolved PanSTARRS1 Sources: Application in the ZTF Real-time Pipeline". In: 130.994, p. 128001. DOI: 10.1088/1538-3873/aae3d9. arXiv: 1902.01935 [astro-ph.IM].

Tendulkar, S. P. et al. (Jan. 2017). "The Host Galaxy and Redshift of the Repeating Fast Radio Burst FRB 121102". In: 834.2, L7, p. L7. DOI: 10.3847/2041-8213/834/2/L7. arXiv: 1701.01100 [astro-ph.HE].

Tendulkar, Shriharsh P. et al. (Feb. 2021). "The 60 pc Environment of FRB 20180916B". In: 908.1, L12, p. L12. DOI: 10.3847/2041-8213/abdb38. arXiv: 2011.03257 [astro-ph.HE].

Thornton, D. et al. (July 2013). "A Population of Fast Radio Bursts at Cosmological Distances". In: *Science* 341.6141, pp. 53–56. DOI: 10.1126/science.1236789. arXiv: 1307.1628 [astro-ph.HE].

Venkatraman Krishnan, V. et al. (Mar. 2020). "The UTMOST survey for magnetars, intermittent pulsars, RRATs, and FRBs - I. System description and overview". In: 492.4, pp. 4752–4767. DOI: 10.1093/mnras/staa111. arXiv: 1905.02415 [astro-ph.IM].

Wright, Edward L. et al. (Dec. 2010). "The Wide-field Infrared Survey Explorer (WISE): Mission Description and Initial On-orbit Performance". In: 140.6, pp. 1868–1881. DOI: 10.1088/0004-6256/140/6/1868. arXiv: 1008.0031 [astro-ph.IM].

Wu, Q., H. Yu, and F. Y. Wang (May 2020). "A New Method to Measure Hubble Parameter H(z) Using Fast Radio Bursts". In: 895.1, 33, p. 33. DOI: 10.3847/1538-4357/ab88d2. arXiv: 2004.12649 [astro-ph.CO].